ELUCIDATING SNOW HEIGHT FOR AVALANCHE ASSESSMENT THROUGH AUTOMATED DATA PROCESSING FROM A REMOTELY PILOTED AIRCRAFT SYSTEM AND AUGMENTED WITH AN ADVANCED ROAD WEATHER INFORMATION SYSTEM

FINAL PROJECT REPORT

by

Eyal Saiet
University of Alaska Fairbanks

Sponsorship
PacTrans and the University and match by Alaska DOT&PF
for

Pacific Northwest Transportation Consortium (PacTrans)
USDOT University Transportation Center for Federal Region 10
University of Washington
More Hall 112, Box 352700
Seattle, WA 98195-2700

In cooperation with U.S. Department of Transportation,
Office of the Assistant Secretary for Research and Technology (OST-R)

DISCLAIMER

The contents of this report reflect the views of the authors, who are responsible for the facts and the accuracy of the information presented herein. This document is disseminated under the sponsorship of the U.S. Department of Transportation's University Transportation Centers Program, in the interest of information exchange. The Pacific Northwest Transportation Consortium, the U.S. Government and matching sponsor assume no liability for the contents or use thereof.

REPORT DOCUMENTATION PAGE

1. Report No.	**2. Government Accession No.** 01784885	**3. Recipient's Catalog No.**
4. Title and Subtitle: ELUCIDATING SNOW HEIGHT FOR AVALANCHE ASSESSMENT THROUGH AUTOMATED DATA PROCESSING FROM A REMOTELY PILOTED AIRCRAFT SYSTEM AND AUGMENTED WITH AN ADVANCED ROAD WEATHER INFORMATION SYSTEM		**5. Report Date 3/12/2024** **6. Performing Organization Code**
7. Author(s) and Affiliations: **Eyal Saiet, University of Alaska Fairbanks**		**8. Performing Organization Report No.** INE/PacTrans 24.02
9. Performing Organization Name and Address PacTrans Pacific Northwest Transportation Consortium University Transportation Center for Federal Region 10 University of Washington More Hall 112 Seattle, WA 98195-2700		**10. Work Unit No. (TRAIS)** **11. Contract or Grant No.** 69A355174110
12. Sponsoring Organization Name and Address United States Department of Transportation Research and Innovative Technology Administration 1200 New Jersey Avenue, SE Washington, DC 20590		**13. Type of Report and Period Covered** **14. Sponsoring Agency Cod**

15. Supplementary Notes

Report uploaded to: www.pactrans.org

16. Abstract

Remotely piloted aircraft systems (RPAS) and a streamlined photogrammetry process intertwined with an advanced road weather information system (ARWIS) can provide continuous data and information about avalanche precursor conditions. A test case in Atigun Pass, Alaska, above the Arctic Circle, is presented. Wind events that generate large blowing snow quantities are believed to be a significant contributor to avalanches there. RPAS coupled with photogrammetry has been shown to have the potential to improve avalanche risk management. We streamlined the photogrammetry and data processing steps, thereby taking a step forward in unleashing this potential. From an operational and science standpoint, the ARWIS is informative during storms when RPAS cannot fly. Linking RPAS surveys and ARWIS data significantly improves tackling avalanche monitoring challenges. We showed that the ARWIS can monitor blowing snow events and has the potential to serve as a snowdrift monitoring system. Our findings revealed that RPAS surveys can tease out even small changes in snow cover, as well as capture cornice growth and collapse. By coupling RPAS surveys and ARWIS data, we compared two similarly significant blowing snow events; however, only one contributed to significant cornice growth. A comparison of measured temperatures and winds and visual inspection of the snowpack surface showed that extremely cold temperatures and scarred sastrugi surfaces might hinder cornice growth. We also showed that sizeable blowing snow events measured by the ARWIS correlated well with reported avalanches and snowdrifts on the Dalton Highway. Overall, this is the first insight into avalanche precursor conditions in Atigun Pass using an RPAS operated by a ADOT&PF and M&O avalanche forecaster.

17. Key Words Unmanned Aircraft, Snow Avalanche Monitoring, Hazard Mitigation, Photogrammetry		**18. Distribution Statement**	
19. Security Classification (of this report) Unclassified.	**20. Security Classification (of this page)** Unclassified.	**21. No. of Pages**	**22. Price** N/A

Form DOT F 1700.7 (8-72) **Reproduction of completed page authorized.**

SI* (MODERN METRIC) CONVERSION FACTORS

APPROXIMATE CONVERSIONS TO SI UNITS				
Symbol	**When You Know**	**Multiply By**	**To Find**	**Symbol**
		LENGTH		
in	inches	25.4	millimeters	mm
ft	feet	0.305	meters	m
yd	yards	0.914	meters	m
mi	miles	1.61	kilometers	km
		AREA		
in^2	square inches	645.2	square millimeters	mm^2
ft^2	square feet	0.093	square meters	m^2
yd^2	square yard	0.836	square meters	m^2
ac	acres	0.405	hectares	ha
mi^2	square miles	2.59	square kilometers	km^2
		VOLUME		
fl oz	fluid ounces	29.57	milliliters	mL
gal	gallons	3.785	liters	L
ft^3	cubic feet	0.028	cubic meters	m^3
yd^3	cubic yards	0.765	cubic meters	m^3
	NOTE: volumes greater than 1000 L shall be shown in m^3			
		MASS		
oz	ounces	28.35	grams	g
lb	pounds	0.454	kilograms	kg
T	short tons (2000 lb)	0.907	megagrams (or "metric ton")	Mg (or "t")
		TEMPERATURE (exact degrees)		
°F	Fahrenheit	5 (F-32)/9 or (F-32)/1.8	Celsius	°C
		ILLUMINATION		
fc	foot-candles	10.76	lux	lx
fl	foot-Lamberts	3.426	$candela/m^2$	cd/m^2
		FORCE and PRESSURE or STRESS		
lbf	poundforce	4.45	newtons	N
lbf/in^2	poundforce per square inch	6.89	kilopascals	kPa

APPROXIMATE CONVERSIONS FROM SI UNITS				
Symbol	**When You Know**	**Multiply By**	**To Find**	**Symbol**
		LENGTH		
mm	millimeters	0.039	inches	in
m	meters	3.28	feet	ft
m	meters	1.09	yards	yd
km	kilometers	0.621	miles	mi
		AREA		
mm^2	square millimeters	0.0016	square inches	in^2
m^2	square meters	10.764	square feet	ft^2
m^2	square meters	1.195	square yards	yd^2
ha	hectares	2.47	acres	ac
km^2	square kilometers	0.386	square miles	mi^2
		VOLUME		
mL	milliliters	0.034	fluid ounces	fl oz
L	liters	0.264	gallons	gal
m^3	cubic meters	35.314	cubic feet	ft^3
m^3	cubic meters	1.307	cubic yards	yd^3
		MASS		
g	grams	0.035	ounces	oz
kg	kilograms	2.202	pounds	lb
Mg (or "t")	megagrams (or "metric ton")	1.103	short tons (2000 lb)	T
		TEMPERATURE (exact degrees)		
°C	Celsius	1.8C+32	Fahrenheit	°F
		ILLUMINATION		
lx	lux	0.0929	foot-candles	fc
cd/m^2	$candela/m^2$	0.2919	foot-Lamberts	fl
		FORCE and PRESSURE or STRESS		
N	newtons	0.225	poundforce	lbf
kPa	kilopascals	0.145	poundforce per square inch	lbf/in^2

*SI is the symbol for the International System of Units. Appropriate rounding should be made to comply with Section 4 of ASTM E380.
(Revised March 2003)

TABLE OF CONTENTS

LIST OF FIGURES

LIST OF TABLES

LIST OF ABBREVIATIONS

API:	Application programming interface
APSIR:	Avalanche Photogrammetry Snow Information Retriever
ARWIS:	Advanced road weather information system
ADOT&PF:	Alaska Department of Transportation and Public Facilities
CP:	Control point
dDEM:	Differential DEM
DEM:	Digital elevation model
GCP:	Ground control point
GNSS:	Global Navigation Satellite System
GPS:	Global Positioning System
GSD:	Ground sampling distance
LiDAR:	Light detection and ranging
LWC:	Liquid water content
M&O:	Maintenance and Operation
MP:	Milepost
NIR:	Near-infrared
NOAA:	National Oceanic and Atmospheric Agency
PacTrans:	Pacific Northwest Transportation Consortium
PCA:	Principal component analysis
RTK-GPS:	Real-time kinematic, Global Positioning System
RPAS:	Remotely piloted aircraft
SAR:	Synthetic aperture radar
SDM:	Snow depth maps
SfM:	Structure from Motion, a similar process to photogrammetry
SZ:	Start zone
TLS:	Terrestrial LiDAR scanner
WSDOT:	Washington State Department of Transportation

ACKNOWLEDGMENTS

This project was largely successful because of the Alaska DOT&PF avalanche forecaster, Mr. Gordon Scott, who went above and beyond conducting the remotely piloted aircraft surveys, supporting the advanced remote weather information system (ARWIS) station, and sharing his insight and knowledge. Also, thanks to Mr. Michael Lilly (GWS) for installing, and supporting, the ARWIS station in such a remote location. I have great appreciation for Alaska's DOT&PF commissioner, Ryan Anderson, who supported the project. Thanks to Mr. Jeff Russel, Dalton District Superintendent, for his support and input. Finally, thanks to Mr. Billy Connor, Director of the Arctic Infrastructure Development Center.

EXECUTIVE SUMMARY

Monitoring large avalanche-prone areas in Alaska is particularly difficult because of the remoteness, lack of nearby weather station data, extreme cold, and poor light conditions caused by polar nights and short days. Beltz and McCormack (2019) showed that a remotely piloted aircraft system (RPAS) coupled with photogrammetry has the potential to aid avalanche risk assessment. However, they also found many challenges, including operating the RPAS, dealing with survey equipment, the photogrammetry and data processing workflow, and the limited light in winter, inhibit the photogrammetry technique. These challenges impede RPAS coupled with photogrammetry from becoming an operational solution. Therefore, we propose that by removing barriers, RPAS coupled with photogrammetry can be adapted as a viable tool.

To this end, we worked at removing as many roadblocks as possible. We focused on building an RPAS flight plan database and streamlined the data processing workflow by building the Avalanche Photogrammetry Snow Information Retriever (APSIR) in-house software. APSIR autonomously processes new RPAS data and manages the photogrammetry processing steps, yielding snow-height information maps. The program also analyzes snow height and keeps track of snow height in critical areas such as near cornices prone to induce avalanches. Agisoft Metashape's application programming interface (API) is at the heart of the software. It is a well-established photogrammetry software. Metashape generally requires knowledge of photogrammetry and geospatial information to operate the software. However, APSIR manages entirely the photogrammetry process. The software also uses Python's open-source rich geospatial packages for data analysis and to create informative figures. APSIR handles all the steps from processing the RPAS imagery to generating informative thematic maps. However, we found that operating the RPAS still required significant effort and that sporadic RPAS surveys, because of weather and limited sunlight, provided only episodic snapshots of current conditions.

We increased the monitoring frequency of avalanche-prone conditions by installing an advanced road weather information system (ARWIS) on the south side of Atigun Pass. The ARWIS location was chosen to be on an exposed ridge, close to avalanche-prone couloirs and in proximity to the Dalton Highway. The ARWIS included hardware proved to operate in the extreme winds, cold temperatures, and moisture conditions typical of Atigun Pass. In addition to standard meteorological sensors, the station had sensors to measure snow height and snow

surface temperature and two FlowCapt sensors to measure blowing snow. The ARWIS operated on solar panels and a power bank only.

Our analysis evaluated how light and snow surface textures varied in time and space. In early January, light was insufficient to identify distinct features in the snow, but by early February, the snow was bright and rich in texture. However, the texture was not consistent with the gain in sunlight. New snow and a lack of wind, particularly in gullies, rendered a smooth snow surface that lacked distinct features and made for weak photogrammetric representations of these areas. However, our analysis of the photogrammetry products (digital elevation models (DEM) and point clouds) using ground control points (GCPs) and sampling the highway below the couloir found an error of about 19.2 cm and 7.2 cm when two large negative outliers were omitted.

Analysis of the ARWIS data was consistent with our observations of the wind regime on the south side of Atigun Pass. We found that winds greater than 5-7 m/s generally originated from the NE-E and that these winds were responsible for most of the blowing snow events. We coupled our analysis of the RPAS surveys and ARWIS data in the timespan of early February to mid-April 2022. During this time, the ARWIS measured only one significant snowfall event of about 25 cm between March 3rd and 6th. That relatively thick snowpack on the ridge lasted only a few days before being obliterated by easterly winds of 8-10 m/s that created only a small blowing snow event. However, two of the most significant blowing snow events between February and April occurred when only a few centimeters of snow were measured by the ARWIS on the ridge. Therefore, we concluded that a significant amount of snow (>20 cm) on the ridge was not required for the sizeable blowing snow events.

We then used the RPAS survey data to investigate the two significant and one small blowing snow events and their impacts on couloirs 115 and 112. Both couloirs had a large cornice along the easterly (windward) side of the couloir. The two large blowing snow events were February 5th-7th and March 8th-12th; the small one was on March 6th. The ARWIS recorded winds of about 12-14 m/s on February 5th-7th and March 7th-12th, respectively, but very different temperatures. During the February event, temperatures were around -35C, whereas during March 8th-12th, temperatures were around -22.5C. Our analysis showed that the wind directions and durations were similar, but the measured blowing snow in February was almost double that of the March event. We used a cross-section tool to tease out the fine-scale changes,

and then we compared our analysis with changes seen on the 2D raster layers. We found that between March 7th-13th (the RPAS survey dates), the cornice at couloir 115 grew the most that season and by a single wind event (about 1 meters). However, when we investigated the impacts of the February 4th-8th wind and blowing snow, we found little change to the cornice size but a significant increase in snow height below the cornice. In contrast to couloir 115, couloir 112 was not surveyed right after these two events; instead, the following surveys were conducted on February 11th and March 31st. However, the wind and blowing snow data confirmed no other significant blowing snow events. Consistent with couloir 115, we saw in couloir 112 no noticeable growth during the February wind event; however, it grew substantially during the March 8th-12th wind and blowing snow event. Vast differences in air temperature, surface roughness near the cornice, the availability of fresh snow, and wind pumping could help explain why we did not see cornice accretion on February 5th-8th but did see it on March 7th-13th.

The RPAS surveys, coupled with photogrammetry and combined with continuously measured environmental data, enabled us, for the first time in Atigun Pass, to tease out avalanche precursor conditions, such as cornice evolution, under very cold temperatures and almost unreported in the literature. Therefore, we conclude that increasing the operation of avalanche precursors in Atigun Pass has the potential to improve decisions regarding avalanche risk and when avalanche control is necessary.

Chapter 1 . INTRODUCTION

Western U.S. states with mountain road passes are often impacted during winter by avalanches with little warning. Limited avalanche precursor information, such as snow depth or relevant wind measurements, makes avalanche risk assessment particularly challenging and biased. This is a significant challenge in large areas, such as Alaska's Turnagain Pass, Thompson Pass, and Atigun Pass.

In the entire state of Alaska, the Alaska Department of Transportation and Public Facilities (ADOT&PF) employs only five avalanche practitioners, and each specialist is responsible for miles of avalanche-prone highway sections. Often, when snow conditions are ripe for an avalanche, many couloirs in a locality will avalanche, overwhelming the ADOT&PF's ability to keep the highway clear and safe for traffic. On average, several dozen avalanches a year block Atigun Pass, usually not hitting a passing vehicle; however, in 2017, one hit four trucks and partly buried one (Daily News-Miner 2017). We assume that other cases go unreported. Sometimes, the avalanche extent is so overwhelming that ADOT&PF closes the road for several days, such as in one case in Thompson Pass in 2014 (Anchorage Daily News 2014). The remote locations of these highway passes, hundreds of miles from a large town, can make removing snow debris a long process in comparison. We propose incorporating measurements of avalanche precursor conditions, such as current snow height or change in snow height, and relevant wind information and blowing snow conditions to aid in the assessment of avalanche risk by making it more data-driven and to increase the safety of the public and M&O staff.

Mapping from aerial platforms has increasingly become more popular. This is attributed to recent advancements in photogrammetry software that enable imagery processing of non-survey-grade cameras. With improvements in photogrammetry and the ability to use off-the-shelf, non-metric cameras, which are orders of magnitude cheaper, the bar to the practice of aerial snow mapping was lowered. Because the location accuracy of such maps is so high, Nolan et al. (2015) were able to demonstrate the ability to derive snow-height maps by using direct geotagging and dual-frequency Global Navigation Satellite System (GNSS) and without relying on ground control points (GCPs). With that, they yielded snow height maps of +/- 30 cm accuracy and a precision that was as good as +/- 8 cm over 5-40 km^2. This proved the accessibility of conducting a snow-height assessment on a large scale at a fraction of the cost of previous surveys.

At first, the adaptation was mostly conducted for academic purposes and from manned aircraft. However, remotely piloted aircraft (RPAS) were becoming ubiquitous at a similar time, enabling airborne photogrammetry to overcome the need for manned aircraft. Eberhard et al. (2021) compared several photogrammetric platforms for mapping snow height and found that the manned and RPAS data were closely aligned, with a root mean square error (RMSE) of only 12 cm. Redpath et al. (2018) demonstrated repeated mapping of snow height in alpine areas with RPAS coupled with photogrammetry to reveal fine changes, such as snow redistribution. In the context of avalanches, Eker et al. (2019) conducted RPAS flights during the summer to yield fine-resolution digital elevation models (DEMs) for modeling avalanche start zones. However, Beltz and McCormack (2019) demonstrated an RPAS coupled with photogrammetry operated by the avalanche practitioner to assess snow height in avalanche-prone gullies on an operational capacity with more than 100 flights!

This project built on the knowledge and infrastructure that Beltz and McCormack (2019) laid and continued focusing on Atigun Pass in Alaska's Brooks Range. The Dalton Highway (brown-colored) crosses the Brooks Range at Atigun Pass (Figure 1.1). The highway connects Alaska's Interior with industry in northern Alaska. The highway enables year-round traffic of both heavy tractor-trailers and private vehicles. These trucks provide critical supply from the mainland to the Arctic coastline.

Atigun Pass avalanches prevent access to the northern sections of the Dalton Highway and the state. ADOT&PF has a Maintenance and Operations (M&O) camp (Figure 1.1), Chandalar Shelf Camp, at the south foothills of Atigun Pass. This M&O camp is dedicated to maintaining highway trafficability between Chandalar Shelf and Atigun Pass. The staff spends many personnel-hours during winter keeping Atigun Pass open to traffic. Much of the M&O staff activity in winter involves removing avalanches or snowdrift debris from the highway.

Figure 1.1. The Atigun Pass study area in northern Alaska. *T*he Dalton Highway is a longitudinal highway connecting Interior Alaska with the Arctic Ocean. The road crosses the Brooks Range in Northern Alaska, above the Arctic Circle.

Beltz and McCormack explored using RPAS coupled with photogrammetry in Atigun Pass to monitor avalanche-prone couloirs. The authors showed the potential of these tools to assist in avalanche risk assessment. The study distilled guidelines and tested them with an ADOT&PF avalanche practitioner to routinely fly an RPAS alongside mountain slopes and collect imagery to use for a photogrammetry process. An experienced spatial data analyst processed the images using Agisoft Metashape, a photogrammetry software, and after a multi-step process, produced a map depicting snow heights. An agreement of about <10 cm was found when snow height maps were compared with manual snow-probe measurements. The photogrammetry product also provided snow volume metrics of couloirs, which can assist in evaluating the risk to the highway below and in determining whether mitigation actions are necessary. However, the study found some challenges in using RPAS coupled with photogrammetry. The study pointed out that because of the nature of photogrammetry, it depends heavily on sufficient light, which makes photogrammetry a limited solution for Arctic regions. The best results were captured under direct sunlight, which is absent during the Arctic polar nights and short days. Furthermore, a lot of skill and experience are involved in safely flying an RPAS over mountains.

Overlooked were the number of M&O hours spent operating the RPAS and surveying the couloirs. The biggest challenge was the multi-step process reported by the study, which was handled remotely by a geotechnical specialist. The multi-step process included the following:

1. Creating flight plans for the desired area of interest.
2. Professionally operating the RPAS camera.
3. Depending on the spatial accuracy requirements, operating survey equipment.
4. Ingesting sensor data into the software and processing the data into a DEM.
5. Deriving absolute snow height values by subtracting a snow-captured DEM from a snowless one.
6. Tailoring the snow height figure to make it meaningful.

In this project, we proposed removing several of the manual steps mentioned above. We suggested creating a flight plan database for all relevant couloirs, reducing the manual labor and expertise of creating flight plans over mountain slopes. We proposed permanent camera settings for avalanche snow monitoring. We also proposed utilizing the ADOT&PF survey crew during the off-season to survey known points. To address points 3 through 6, we proposed building hands-off software to process the RPAS imagery into easily readable snow height maps. The software, APSIR (Automatic Photogrammetry Snow Information Retrieval), would organize the data and make them easy to transform into products. APSIR would require only basic computer skills. We hypothesized that RPAS data and information, such as snow height maps, would be readily available by minimizing the manual steps. Furthermore, we believed that routine RPAS surveys would likely capture the snow conditions in couloirs both before and after avalanches had occurred. Capturing such a sequence of events could improve our understanding of avalanche dynamics, both in individual couloirs and in the local mountain pass.

Even with streamlining the RPAS-coupled photogrammetry data processing, the method would still be heavily dependent on direct sunlight conditions. Also, avalanches often occur during blizzard conditions, which render an RPAS coupled with a camera useless at assessing snowpack conditions. To mitigate these challenges, we proposed installing an advanced road weather information system (ARWIS) for continuous data collection and real-time reporting during non-flyable blizzard conditions. The ARWIS should be close enough to monitor the conditions in the nearby couloirs. The intent would be to continuously measure blowing snow and other avalanche-prone conditions near couloirs from the onset of a blizzard until the

conditions diminished. Routine RPAS surveys during bluebird days, outside of storms, combined with continuous ARWIS observations during blizzard conditions were hypothesized to provide a more comprehensive picture of snowpack conditions and to aid in assessing avalanche risk.

We anticipated additional benefits beyond assessing avalanche risk by installing an ARWIS near Atigun Pass. One of them would be to have real-time, in-situ monitoring of winter hazard traffic conditions. The new data and some data assimilation of snowdrifts and whiteouts could improve safety for highway users and increase M&O staff's situational awareness when they were not on site. Snow drifts are a frequent driving hazard throughout the winter in Atigun Pass. M&O staff monitor Atigun Pass trafficability throughout the day by traversing the pass. However, there are long periods of time during the day, and more so at night, when M&O staff are not at the pass (e.g., at camp), and it is during this time that snowdrifts may be stacking to dangerous heights. Thus, there would be value in an AWRIS continuously monitoring the potential of snowdrift severity.

We hypothesized that by improving the data and information about avalanches and snowdrifts, the M&O staff could be more strategic in their response efforts.

Chapter 2 . BUILDING THE RPAS AND ARWIS DATA PROCESSING PIPELINE

This chapter discusses the buildup of two key project components, the RPAS photogrammetry data processing pipeline and ARWIS and data analytics. During the project, the RPAS flights were focused on the south side of Atigun Pass because of frequent avalanches and better sunlight exposure. All couloirs in Atigun Pass have identification numbers to aid communications. This project focused on two avalanche-prone couloirs, 112 and 125 (Figure 2.1). Out of about 70 avalanches in 2019-2020, about half were in couloirs 112 and 125. Couloir 115 is not an avalanche risk to the highway but was proposed as analogous to couloirs 112 and 125 and a study site to test methodologies. The ARWIS was about 50 meters northeast of Couloir 115.

The perimeters of the three couloirs are labeled black in Figure 2.1. These perimeters were used to create the RPAS flight plans and were part of the data processing. The data processing workflow kept track of snow height inside these perimeters. These perimeters and other vector files of key locations, such as critical cornices and start zones (SZs), were part of an Atigun Pass database.

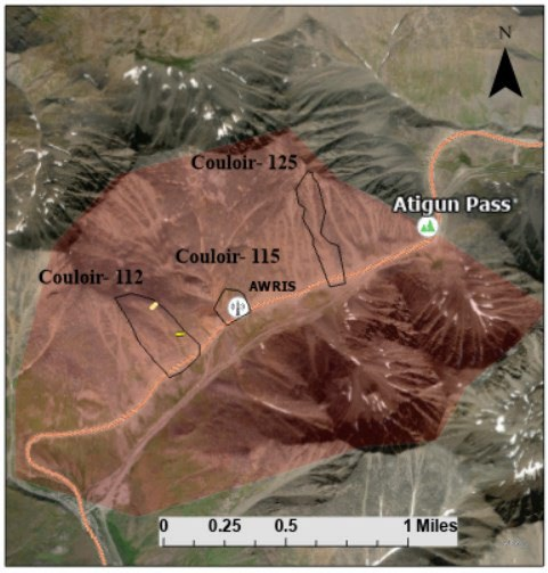

Figure 2.1. The south side of Atigun Pass is highlighted in red, as well *as* the avalanche-prone couloirs and the location of the ARWIS station.

Atigun Pass snowpack typically peaks around May at about 101 cm (40 inches), (NRCS 2024). For a winter season that is about 8 months long (October-May), that is about 12 cm of snow a month. Most of the snow comes from storms from the south, and there is even less snow on the north side of Atigun Pass. Thus, avalanches and road snowdrifts on the south side of Atigun Pass result from snow transport and not from significant snow precipitation. Winds transfer snow, mostly from exposed ridges, downwind, where the snow particles accumulate in couloirs, which are effective snow catchment traps. When the snow in the couloir reaches a critical point, it avalanches. Most blowing snow events result from northeast winds originating from the pass. Couloirs 112, 115, and 125 collect the suspended snow originating upwind. The same blowing snow effect is responsible for drifting snow on the south side of the pass. However, the locations of snow drifts along the road vary.

2.1. ARWIS Station Build-Up

To monitor blowing snow events that induce avalanches and snowdrifts on the highway, we installed the ARWIS at the heart of the south side of Atigun Pass. The location was chosen to be on an exposed ridge to effectively measure the brunt of the winds and blowing snow and to be as close as possible to the nearby avalanche-prone couloirs. Its placement also had to be out of avalanche paths. The site was also within 40 yards from the Dalton Highway, and the hope was that the station measurements would accurately represent the highway's blowing snow exposure.

The site and the ARWIS station, as well as the views in both directions, are depicted in Figure 2.2. In Figure 2.2 on the left panel, looking northeast, one can notice Atigun Pass in the distance and where the winds that generate blowing snow originate. One can also notice the highway below the station.

Figure 2.2. Left: Picture of the ARWIS orientated northeast, with Atigun Pass at the top. Right: Picture of the ARWIS-oriented southwest, with the 115th behind the ARWIS over the edge.

Ridges on the south side of Atigun Pass endure continuous winter cycles of snow accumulation followed by northeast winds stripping the snow down to the bare ground. The heterogeneity in the amount of snow cover in this landscape due to these winds is depicted in both images in Figure 2.2; in looking northeast up toward the pass (left panel), one can see the surface mostly covered in snow. These are the areas protected from the northeasterly winds. In looking at the image on the right, aiming southwest, one sees more areas of bare earth (less snow). The bare-earth areas, as well as the station site (which has little snow), are subject to strong, frequent northeast winds. The near snow-free ground and snow erosion features below the ARWIS indicate a previous wind-driven snow erosion event.

In addition to the ARWIS location considerations, significant effort was put into building the ARWIS station. The goal of the ARWIS was to monitor the northeast winds that are responsible for the bulk of avalanches and the snowdrifts on the Dalton Highway on the south side of Atigun Pass. To collect the critical data and communicate them from a remote and harsh site, certain considerations were necessary.

2.1.1. Hardware

All components were selected on the basis of their proven track record at operating in harsh weather conditions. The station sensors were primarily installed on a rigid tripod and a nearby mast (Figure 2.3). The wind was the chief environmental variable of concern. Therefore, two anemometers were installed for redundancy. One of them was designed for the mountainous environment and was, in general, beefier. A few snow-specific sensors were also installed, including two FlowCapt sensors that measured blowing snow and sensors to measure snow height. In addition, two hardened cameras with integrated near-infrared lamps and a defrosting thermistor were part of the station. One camera pointed toward the northeast, the top of the pass, and the other camera pointed southwest, near the base of couloir 112.

The ARWIS operated off-grid, without a generator and without cell service. The station ran on a solar panel and a large battery bank. The battery bank was large enough to sustain the station through more than a month of polar nights and no solar power. The system was connected to an advanced, low-power radio system that enabled sending the data to the M&O camp about 5

miles away. The radio system provided a burst of data every 15 minutes and nearly real-time measurements from the site.

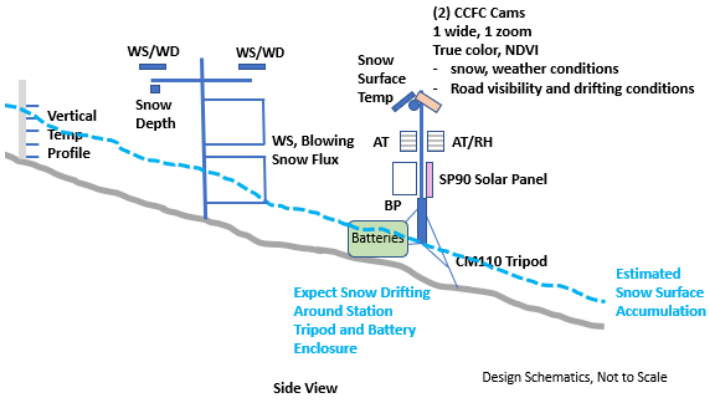

Figure 2.3. A diagram of the ARWIS station and components.

2.1.2. Software

The software that ran on the ARWIS datalogger was written and tailored for this site and the station's specific objective. It managed the station sensors, telemetry radio, and cameras to minimize power requirements. The software created different data files for different end-users and analyzed the incoming data in real time. If certain conditions were met, the system would react. For example, if wind conditions passed a certain threshold, then the snow-height measurement frequency and picture-capturing rates increased.

2.1.3. Data Output

The ARWIS was built to serve multiple end users, from M&O crew to regional transportation needs, as well as National Oceanic and Atmospheric Agency (NOAA) forecasters, weather models, and the data requirements for this project. The data logger recorded different combinations of sensor data at different time intervals based on the needs of each end user.

Ease of access to the ARWIS data was a chief concern. The primary goal for the ARWIS was to serve the M&O staff in their daily effort to keep traffic safe on the road. Data from the ARWIS were transmitted to a dedicated computer at the M&O camp. The data could be viewed through various websites, even when the Internet connection to the outside world was disrupted. The data were stored and backed up. The data on the computer at the camp often represented ARWIS observations from the past 15 minutes.

Generic data, such as temperature, wind, relative humidity, and air pressure, are posted on the Alaska DOT&PF 511 website, https://511.alaska.gov/. The 511 website compiles road and weather conditions across the state, enabling regional ADOT&PF, private, and commercial users to make decisions about travel and roadway management.

Some of the data are also synchronized with MesoWest, https://mesowest.utah.edu. MesoWest is a hub of thousands of weather stations nationwide. The data are publicly available and updated within a few hours. Many weather forecasting models use data from MesoWest. Having a station near the pass reporting current conditions improves the weather forecast accuracy for that area.

In addition to the generic data published on the state's 511 and MesoWest websites, more specific data are posted on a dedicated website. Data on this site focus on specialized end users, such as the M&O staff, NOAA weather forecasters, and ARWIS maintenance. The site pulls data from a remote server that stores and backs up the data at the Chandalar Shelf M&O camp. The website depicts three main categories of information: weather, snow, and the station's diagnostics. Under each category, one can investigate current and historical data from up to a year before. Higher frequency data for research purposes, such as this project, are also collected and stored on a local computer.

2.2. Streamlining RPAS Photogrammetry Data

M&O staff, such as the avalanche practitioner responsible for Atigun Pass road safety, are based at Chandalar Shelf. When required, the avalanche practitioner drove to the bottom of a nearby avalanche-risk couloir to launch the RPAS and survey the couloir of interest. After conducting the survey, the avalanche practitioner returned to the M&O camp and downloaded the data on a dedicated server.

From there, the manually intensive skill required to process the RPAS imagery into snow-height information was replaced by the APSIR software we built for the project. The APSIR software would complete all the geospatial manual steps and avoid any chances of human error. There were some cloud-based solutions available, but none could provide the complete process that APSIR offered. Also, cloud-based solutions depend on reliable, high-bandwidth networks to upload the RPAS data and download the resulting products. However, the unreliable and low-bandwidth Internet connectivity at the M&O Chandalar Camp was too inadequate for a cloud solution to be even considered. The availability of photogrammetry software that could be

incorporated as a component into our self-built software and the proliferation of open-source Python scripting tools encouraged us to explore building our own software to complete the entire required process.

A streamlined data processing pipeline depends on consistent data types and, in the geospatial context, consistent coverage. For example, the circumference of the couloirs depicted in Figure 2.1 was the expected minimum coverage for all RPAS surveys of that couloir. In fact, it also prevented the RPAS operator from creating flight plans that exceeded the area of interest, which would have added unnecessary aircraft flight time. Upholding this consistency enabled the streamlined processor to process the data with minimal error and a comparison of the products with past ones. This comparison provided more insight into couloir avalanche dynamics.

Data consistency was improved through a design for repeatable flights. The couloirs in Atigun Pass are numbered, and their perimeter was digitized at an early stage of the project. The intent was to have a particular flight plan for each couloir. Some longer couloir surveys required more than one battery. When avalanche practitioners had limited time, they might survey only the upper part of the couloir, such as the SZ.

It is difficult to fly an RPAS safely in the Arctic, over a mountainous environment near steep slopes, at high elevation, and with strong sustained and gusty winds. At the same time, the road nearby is open to traffic. Added to the challenges are the limited places from which to launch the RPAS on a road with ongoing traffic. This made a case for use of a robust flight plan, GNSS, and an autopilot that could safely handle these challenges and minimize human error. Unfortunately, the RPAS that was used, the DJI Phantom 4 RTK, could not fly high enough above the takeoff location, which prevented the aircraft from mapping the upper reaches of the couloir. Therefore, some manual RPAS flying was needed, which increased the chance of human error.

Much consideration was given to easy access to the data products and the storage hierarchy structure. M&O staff have limited time to delve into files. The data structure was designed such that the products could be obtained with ease. After each RPAS survey, the data, images, and GNSS information were stored in a new folder with a consistent description of the survey in a folder that contained all previous couloir surveys. Products were stored both in the relevant survey folder and in a dedicated couloir-product folder. For example, couloir- “x” would

have a product folder for all survey products of the relevant season. Consistent data organization allowed the APSIR to compare a recent snow height value with values from a previous season.

Given everything mentioned above, we built the data processing program—APSIR. After the RPAS pilot completed the survey, they downloaded the data into a new folder in the dedicated computer. From there, the software took over execution of the following steps (summarized in Figure 2.4):

1. APSIR checks for unprocessed datasets or multiples and creates a queue to process each.
2. Several intensive steps are taken before the photogrammetry process. These steps include creating and organizing files needed for the photogrammetry process and verifying the presence of the vector files used to define the area of interest and to calculate analytics of the targeted sites within the area of interest, such as a cross-section of a cornice.
3. APSIR manages the photogrammetry processing steps, makes sure that they are consistent, and creates the desired product files.
4. Following the photogrammetry step, APSIR retrieves a snowless DEM of the couloir and uses it to calculate snow height values.
5. Using a vector database APSIR also calculates snow height and volume metrics and summarizes the changes in a table.
6. Absolute snow height and relative changes in snow height based on the existence of a previous survey in the database are calculated and depicted by carefully adjusting color maps to best depict the changes on a thematic map.

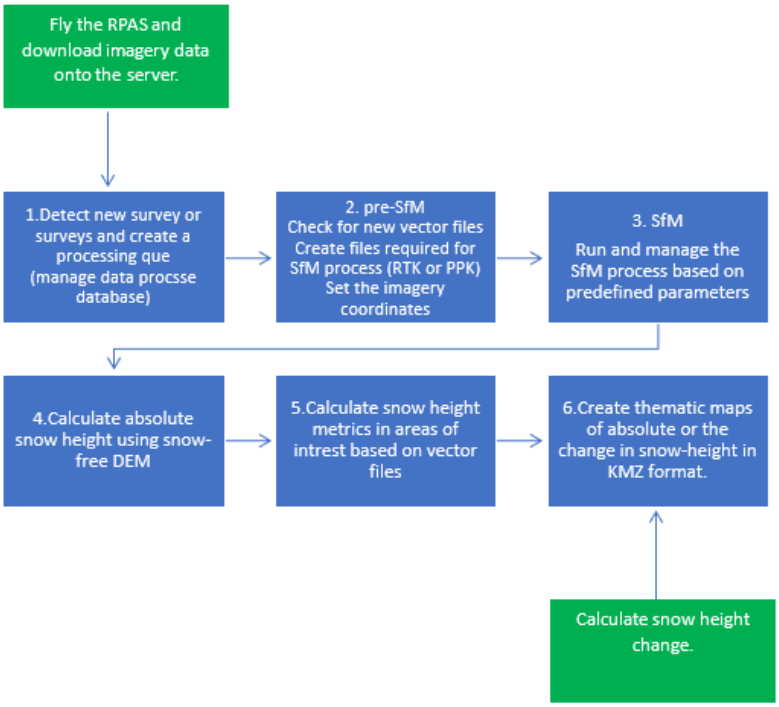

Figure 2.4. This is a high-level diagram of the APSIR data processing workflow. The green boxes at the start and end depict the means of providing input to the process.

At the end of the photogrammetry step, APSI saves the relevant data in a new products folder, as discussed earlier. In the products folder are the photogrammetry required files and products in various file formats (Figure 2.5). The products are the orthomosaic and DEM in a TIF format to be read by any geospatial software. The orthomosaic is in a KMZ format that is more user-friendly and can be viewed in the Google Earth tool.

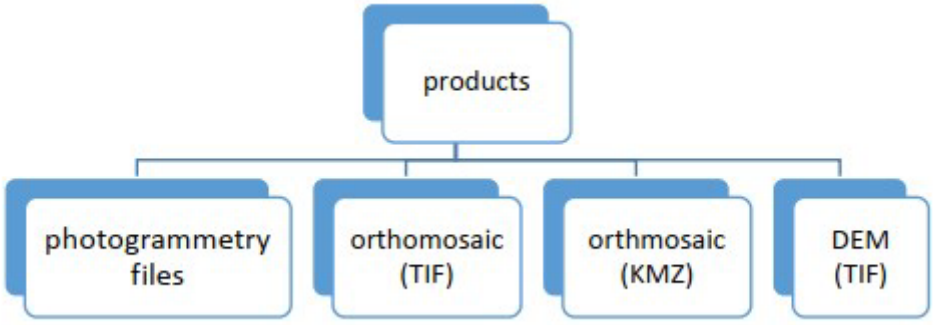

Figure 2.5. An example of the APSIR products output and data hierarchy.

After completing the photogrammetry step and yielding the photogrammetry products in the product folder, the APSIR moves on to analyze the products, and it uses other available data

(snow-less DEMs and local vector files). The analysis information is then placed in an analysis folder (see Figure 2.6). In the analysis folder, raster files that are part of the calculations are saved as TIF files. The informative analysis outcomes are thematic maps. The thematic maps are carefully colored maps that highlight specific absolute snow heights, changes in snow height, and more. The thematic maps are saved as jpeg or KMZ files. Both can be viewed by free and readily available software. The KMZ and jpeg files are compressed formats. The jpeg image is compressed in a lossy compression, and the KMZ is a PNG with a lossless compression. The compression of both files makes sending the files via email or another method easier than sending a large TIF file.

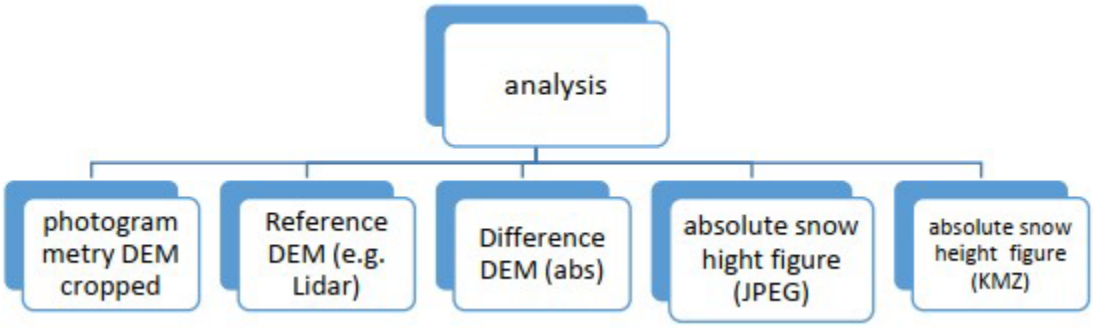

Figure 2.6. A diagram of the APSIR analysis folder and data structure.

Chapter 3 RESULTS AND ANALYSIS

During this project, more than 24 RPAS surveys were conducted over Atigun Pass. The bulk of the RPAS flights spanned from January 10 through April 29, 2022, capturing couloirs 112, 115, and 125 on the south side of the pass. Two surveys of couloir 306, on the north side of the pass, were collected between May and early June. The avalanche practitioner conducted the flights based on available time and favorable flying conditions. The ARWIS has been collecting data since October 2021, more than two years, and is still ongoing.

3.1. Overview of RPAS Photogrammetry Products

The RPAS flights spanned over six months and depicted drastic light gain in the region. A summary of the flights is seen in Table 3.1. All surveys were processed entirely by the APSIR software with no manual intervention. APSIR created products and analysis files for each processed survey, as described earlier.

Table 3.1. Summary of RPAS flights during the winter-spring of 2022.

Couloir	10-Jan	11-Jan	4-Feb	8-Feb	11-Feb	15-Feb	3-Mar	7-Mar	31-Mar	12-Apr	28-Apr	29-Apr	30-Apr	7-May	30-May	2-Jun	Sum
112			1		1		1	1	1	1		1					7
115	1	1	1	1	1		1	1	1			1					9
125						1			1	1	1		1	1			6
306															1	1	2
																	24

Couloir 115 was first surveyed on January 10th and the last flight was on April 29th. Significant changes in light were observed during this period. Because the RPAS collects imagery for a photogrammetry process, changes in light play a significant role in the data quality. Figure 3.1 depicts dramatic light gain over the study period.

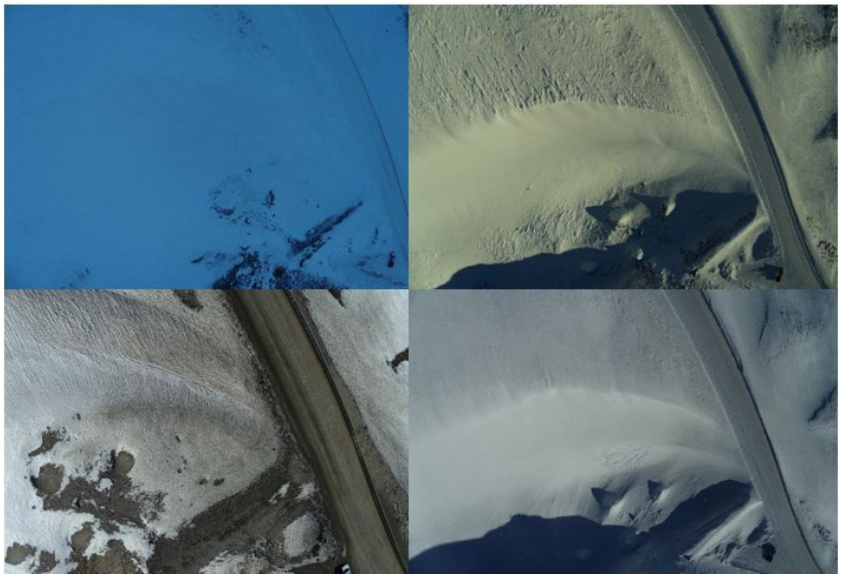

Figure 3.1. A collage of four RPAS pictures. From the top left and clockwise: January 11th, February 4th, March 7th, and April 29th.

Figure 3.1, from the upper left panel clockwise, shows the brightness gained on the snow and the changes in the color pallet: from dark blue to yellow to bright white. Also seen is the gain and diminishment of shadows. There are noticeable changes in shadows: low light and no shadows, to the presence of the shadows on February 4th, to the diminishment of shadows by April 29th. The shadows' evolution and the increase in brightness are signs of the increasing sun angle between the RPAS surveys. While there was consistent gain in brightness and color change during the study period, texture varied between the surveys. On January 11th, the image was flat or of poor contrast, with insufficient light to spot features in most of the scene; on February 11th, there was better light and an abundance of distinct snow features, but mostly snow-eroded features due to wind. But on March 7th, there was a loss in distinct features. Consistently, there, the gully and hillside were featureless. This hillside, shadowed by the wind, lacked snow erosion features, resulting in a smooth and featureless surface. By April 29th, there were noticeable features in the gully due to melting streaks. The lack of distinct features played a significant role in the data, as can be seen in Figure 3.2. This figure depicts the sparse point cloud, representing all the distinct features in the surveyed area, as captured on January 10th. Where there were few tie points there was a large cavity (highlighted in red) in the sparse point cloud data. This was mainly where snow was collected, which was a crucial area for avalanche analysis.

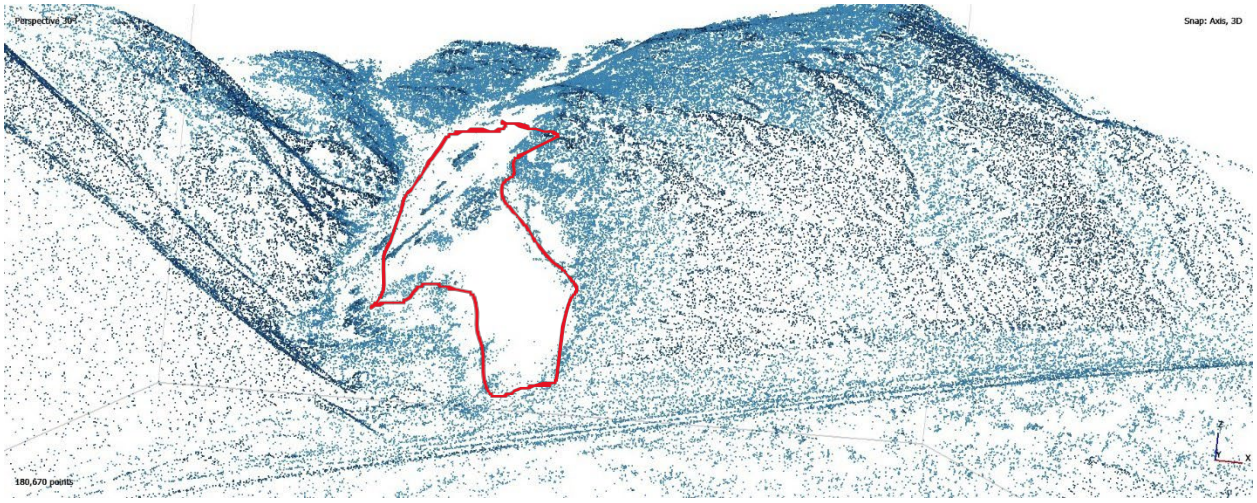

Figure 3.2. The sparse point cloud of couloir 115 as captured on January 10th. The red line highlights the cavity in the data due to a low number of tie-points.

There was an increase in detail by February 4th, as seen in the sparse area in Figure 3.3. Here, the gully was better mapped with a higher number of tie points. But there a cavity still existed (bounded in a red line).

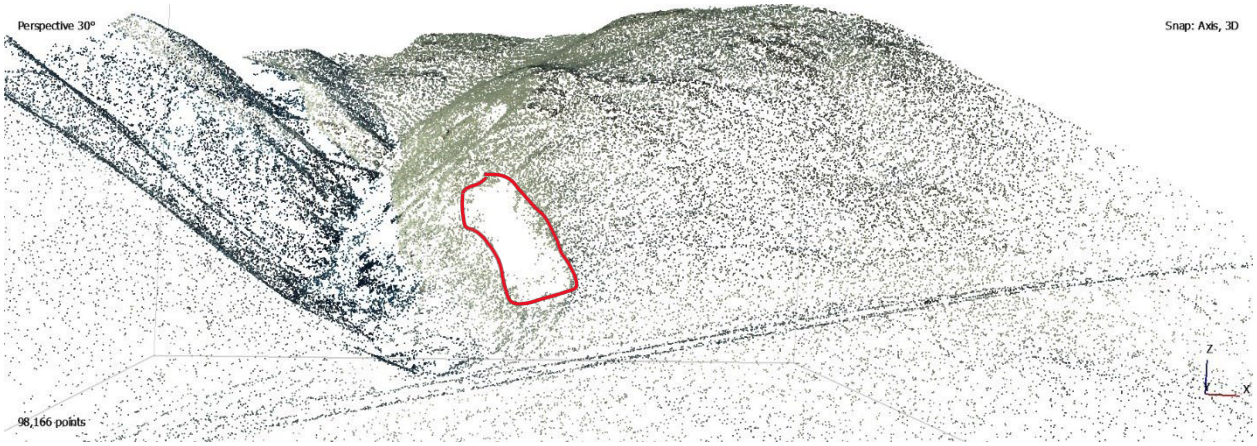

Figure 3.3. The sparse point cloud of couloir 115 as captured on February 4th.

Despite the increase in light by March 7th, a smoother surface due to new snow and the presence of the shadow in the valley created a larger cavity in the data (Figure 3.4).

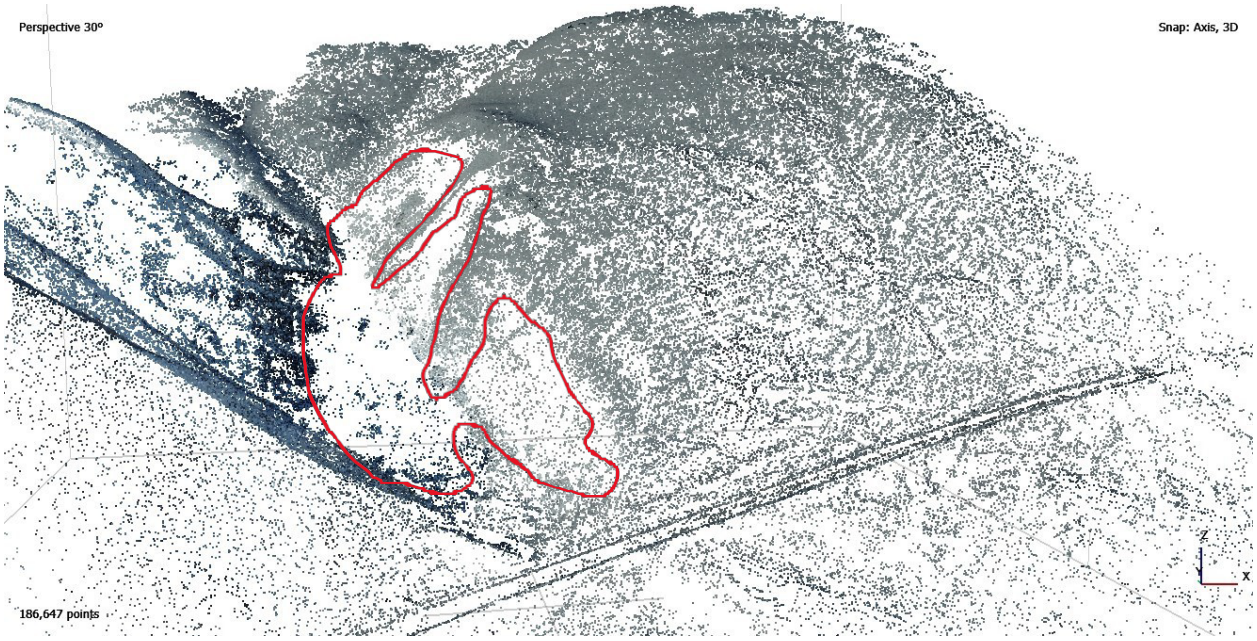

Figure 3.4. The sparse point cloud of couloir 115 as captured on March 7th.

The low number of tie points in the gully and the windward sidehill resulted in large voids. The Metashape photogrammetry software filled the voids by using interpolation. By default, Metashape fills the voids by using interpolation unless instructed otherwise. Without the software filling these voids, it would be difficult to assess snow conditions in the gully. However, it is unknown how representative that interpolation is, particularly in areas of steep change in elevation, such as a sidehill.

The APSIR software assessed the product accuracy of surveys that included a section of the highway. The assessment was done automatically by two different means: using a ground control point (GCP) on the side of the road and sampling points along the road. The GCP was a temporarily mounted ground control on a pre-mounted receiver on the guardrail. The GCP was placed on the guardrail before the RPAS flight. A database of all GCP locations was used to analyze product errors. Generally, adding GCPs was a manually intensive step in the photogrammetry process. The step included manually identifying the GCP in as many survey images as possible. APSIR included a capability in Metashape to find the GCPs automatically. However, this autodetect tool was not robust in most of our surveys. Table 3.2 shows only a few locations where the autodetect worked. In fact, an additional algorithm was needed to make it work even for the locations it did.

In Table 3.2, the “Autodetect” column summarizes when Metashape was successful at automatically identifying the GCP in the scene. However, in many scenes, the software did not

detect the GCP and manual selection was required. The principal failure of the GCP autodetect tool was due to the bright, snowy background and the darker GCP (Figure 3.5). Therefore, the GCP ended up being underexposed and undetectable. In the figure, the top panels have bright snow in the background; therefore, the GCPs were undetected. However, the lower panels are pictures of locations where the GCPs were successfully detected. Darker snow scenes or snow-less backgrounds seemed to be more conducive to GCP autodetect success.

Figure 3.5. A collage of pictures collected from the RPAS of a GCP on the guardrail. From upper left clockwise: February 4th, February 11th, March 3rd, and April 29th. Among the four pictures, only the GCPs at the bottom of the figure were automatically detected by Metashape.

The APSIR product errors using the guard rail GCPs are summarized in Table 3.2. The x, y, and z values in the table represent the offsets between the GCP and the respective location in the data. Because of the avalanche practitioner's limited time, not all surveys included a GCP. Usually, only a single GCP was installed before the RPAS survey. The z root mean square (RMS) offset of all GCPs was 19.2 cm. If the large negative values (-71 and -18 cm) outliers were omitted, then the RMS was even smaller, 7.2 cm.

Table 3.2. A summary of the GCPs' measured offset.

Couloir	Date	# GCP	X Error (cm)	Y Error (cm)	Z Error (cm)	Autodetect
ch-112	22-02	1	-7.8	-0.9	2.8	Manual
ch-112	22-02	1	-6.4	-1.9	0.3	Manual
ch-112	22-03	1	-0.7	-2.4	1.8	Yes
ch-112	22-03	1	-2.6	-3.5	7.1	Yes
ch-112	22-03	0				No marker
ch-112	22-04	0				No Marker
ch-112	22-04	1	1.6	-1.6	1.8	Yes
ch-115	22-1-	1	1.0	2.8	3.6	Manual
ch-115	22-01	0				No marker
ch-115	22-02	2	1.2	1.4	5.7	Manual
ch-115	22-02	2	-1.4	1.5	11.2	Manual
ch-115	22-02	1	-0.9	-3.1	3.6	Manual
ch-115	22-03	1	0.9	-1.7	9.3	Yes
ch-115	22-03	1	0.7	-2.9	8.3	Manual
ch-115	22-03	1	-8.8	-25.8	-71.9	Manual
ch-115	22-03	0				No marker
ch-115	22-04	1	0.4	-7.3	-18.0	Yes
ch-125	22-04	2	2.7	-7.5	-19.1	Yes
ch-306	22-05	2	2.8	6.6	2.2	Yes
ch-306	22-06	2	4.9	7.9	0.4	Yes

For areas where GCPs were unavailable and for redundancy, the APSIR software used the Dalton Highway at the bottom of the couloirs to verify that there were no drastic errors or shifts in the map. To that end, a line of roughly a hundred meters was sampled after each survey. The only exception to that was where only the upper area, the SZ of the couloir, was mapped—excluding the road. The line can be viewed in Figure 3.8 as the red line along the road. Using the snow-height DEM product, the software sampled the road along the charted line. With ADOT&PF generally maintaining the roads, we assumed there would be little snow or ice on the road. The mean and standard deviation of this sampling are plotted in Figure 3.6.

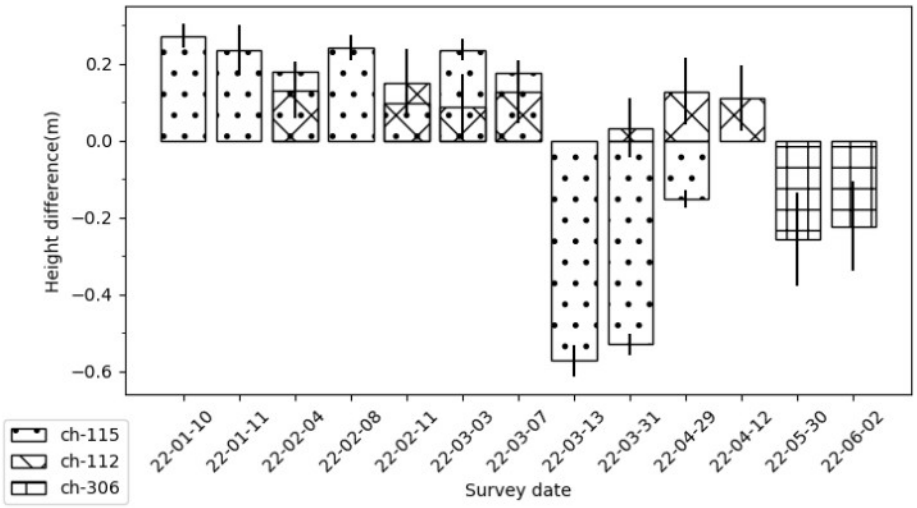

Figure 3.6. A summary of the error analysis using the Dalton Highway at the base of the respective couloir (112,115, and 306).

Generally, the M&O clears most of the snow and ice from the road; however, some is often left. A positive value in Figure 3.6 means that there was some snow on the road during the survey. It is the difference between two surveys with snow and without. However, a negative value means that the DEM from the winter survey was lower than the snow-free one from the summer—which doesn't make sense.

The particularly large and negative values on March 13th and 31st and smaller values on April 29th are suspicious, suggesting some systematic biased error, perhaps with the aircraft GPS system. In fact, there were significant GPS challenges with operating the RPAS safely in the mountains around Atigun Pass, before an RTK system was introduced.

Except for the March 13th and 31st surveys, both the GCPs and the Dalton Highway sampling analysis confirmed that the accuracy of the DEM at the measured location was within +/-20 cm. However, these measurements were along the road, which generally had a relatively denser number of tie points. It is unknown what the error was where the density of tie points was low and voids were filled by interpolation.

Knowing that there were large voids, particularly in the gullies, we handled the analysis in the gullies with caution. An example of the APSIR products and analysis—the orthomosaic and a snow height DEM—is seen in Figure 3.7. The figure depicts couloir 112 as surveyed on March 7th. One can notice the cornice hanging above the couloir. The cornice is well depicted both in the orthomosaic and in the snow-height DEM.

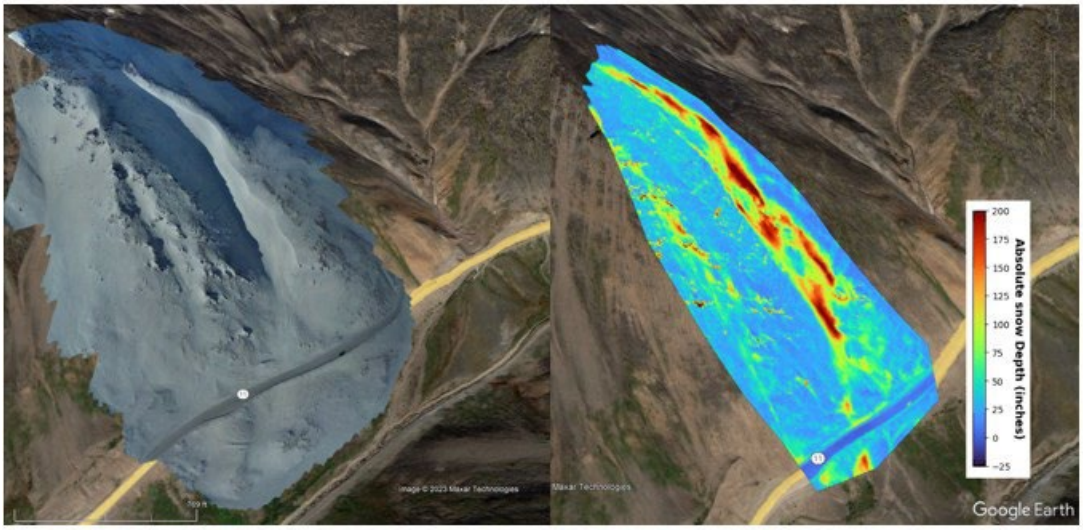

Figure 3.7. March 7th survey products: an orthomosaic (left), absolute snow height calculation (right). Both files are in the KMZ format and are observed in Google Earth.

3.2. Photogrammetry Products Snow Height Analysis

Repeated couloir surveys enable insights on the conducive conditions that lead to avalanches. We used the same tool that is used for analyzing the road surface to analyze cross-sections of the couloirs, particularly the sidehill. The APSIR used vector files within a database to sample the snow height DEM in key areas of interest. Such key areas were the snow conditions in the starting zone (SZ) or a cornice that could initiate an avalanche. The database also included a file for each couloir to calculate snow volume on a road after an avalanche.

Couloir 115 doesn't avalanche on the Dalton Highway; however, because it collects snow downwind from the AWRIS, it was a case study site for exploring snow accumulation, erosion, and avalanche due to snow precipitation, wind, and blowing snow. It was our hope that couloir 115 could serve as an analogy to couloir 112, which does avalanche on the Dalton Highway. The cross-section of the eastern side of the couloir 115 is seen in Figure 3.8 in the two panels. The figure's upper panel depicts the cross-section's spatial extent in orange. The bottom panel depicts the snow surface height (elevation) as captured by the RPAS during the period of January 10th to April 29th. A blue arrow depicts the prevailing strong winds transporting the bulk of the snow.

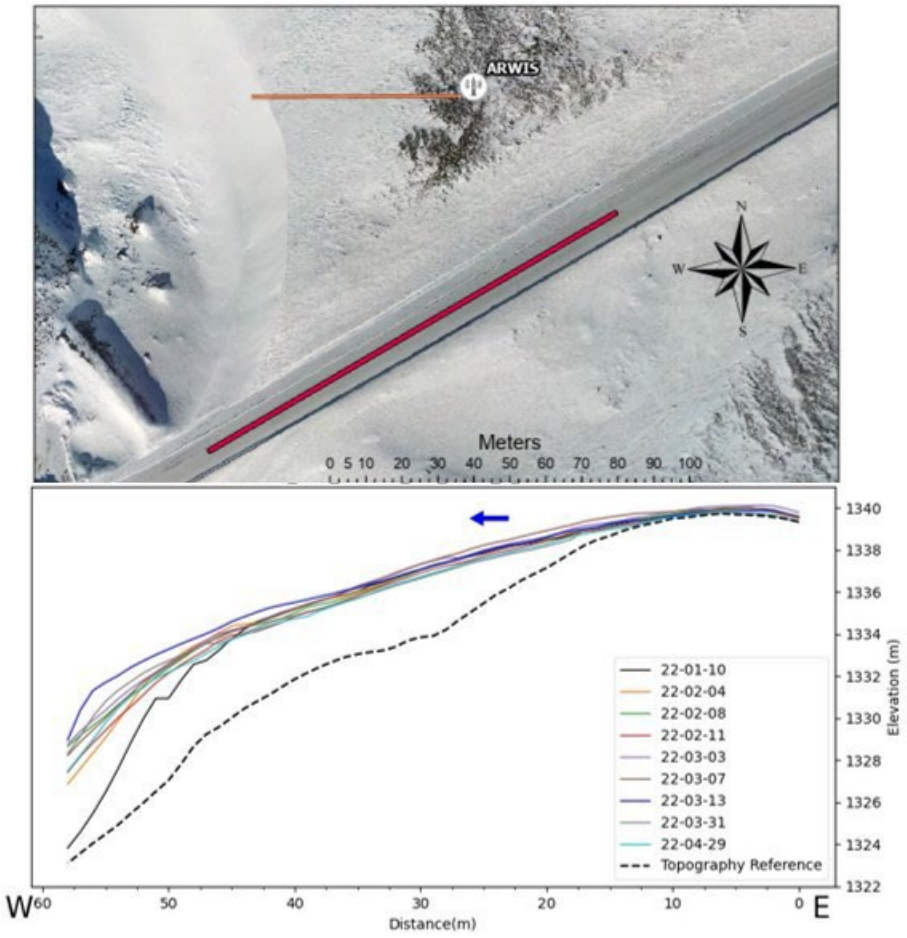

Figure 3.8. Upper panel: The cross-section is in orange, and the road height measurement is in red along couloir 115 over the orthomosaic. Bottom: The stacked DEM cross-section profiles are labeled with the survey collection date. The blue arrow depicts the prevailing strong wind direction.

The dashed line depicts the surface topography captured by a snow-free survey's DEM. Knowing that most of the gullies had large voids filled by interpolation, whereas the ridge above had better tie point distribution, we focused the cross-section analysis on the latter. The cross-section seemed to depict well the snow surface evolution; however, there were no outside means to confirm its accuracy. The April 29th survey was rich in snow-melting streaks in the gully, which provided rich texture and a better distribution of tie points. Thus, the April 29th gully had our highest confidence. The sampling of the cross-section of couloir 115 was done from east to west ("E" to "W"). The eastern side of the plot, also the "zero" value of the x-axis, was the reference for further discussion. The least amount of snow was along the exposed ridge at about 5 meters. There was a bit more snow on the leeward side, about 0-5 meters. Snowpack thickness

increasesd on the leeward side up until the cornice, peaking at upwards of 7 meters of snow (not seen). The stacked snow surface profiles depict the variation in the snow surface height during the period of January 10th to April 29th. The minimal snow height at the edge of the gully was January 10th, with the peak surface height on March 3rd. The cornice on March 13th was hardly noticeable. The exact location is where there was a sharp drop in elevation at about 55 meters from the origin of the x-axis. The 2D raster and the sampling of 1 meter blur the abrupt drop in elevation.

Down the valley from couloir 115 is couloir 112, which prominently avalanches onto the Dalton Highway. Just like couloir 115, a cornice is often built on the northeastern side of the couloir. We used the cross- section tool to analyze the snow profile near the common avalanche start zone. The cross-section extent is marked in orange in Figure 3.9. At that location, the predominant strong winds blow from north to south, which is the direction we sampled.

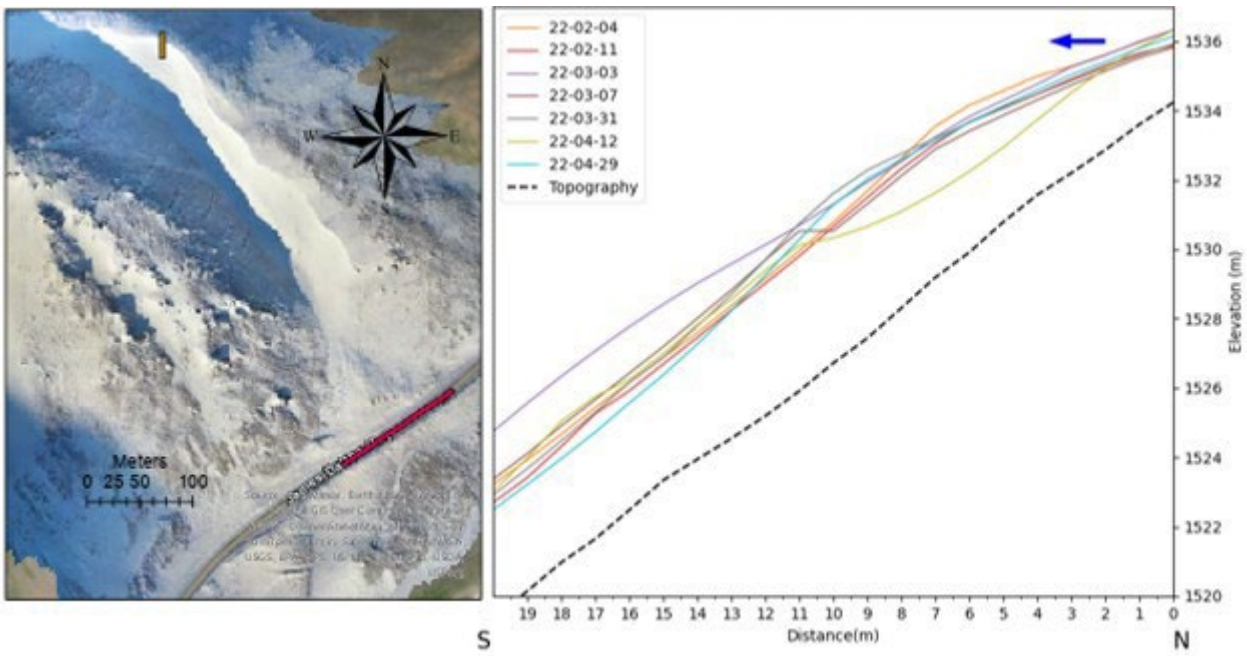

Figure 3.9. The cornice cross-section in couloir 112. Left: The cornice cross-section is orange, and the highway height measurement is in red. Right: The stacked survey surface height cross-section along the cornice. The blue arrow depicts the prevailing strong wind direction.

Figure 3.9 depicts a cross-section at the top of couloir 112. The left panel shows the spatial extent of the cross-section draped on an orthomosaic from the photogrammetry process. On the right are the survey-cross sections labeled with a solid line. A black dashed line marks a

snow-free topography reference. The figure depicts the cornice cycle of growth and collapse. The cornice advanced from February 4th to the furthest extent by March 31st. By April 12th, there was evidence that the cornice collapsed. In some cases, the breakup of the cornice in this part of the couloir results in avalanches that may cover the road below.

Couloir 125 also prominently avalanches onto the Dalton Highway. The sheer elevation difference from the road to the SZ requires two RPAS flights to map the entire couloir. Thus, often when the avalanche practitioner's time is limited, only the SZ is mapped. In Figure 3.10, the snow height is depicted; see the left y-axis. The dashed-black line depicts the topography shape. The blue arrow depicts the prevailing wind that, through blowing snow, loads the couloir.

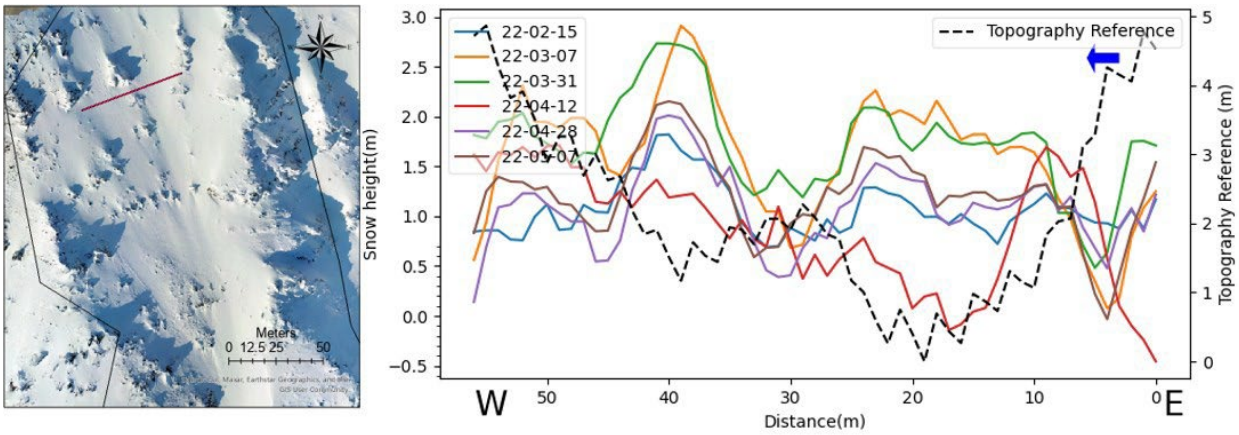

Figure 3.10. Left: Colored in red is the cross-section of the start zone (SZ) in couloir 125. Right: The stacked cross-section of snow-height is labeled with the RPAS collection date. The blue arrow depicts the prevailing strong wind direction.

In cases where only the SZ was mapped without the road, there was no opportunity to check for accuracy by using the GCP on the guardrail or sampling the road. The survey on April 28th had the highest number of tie-points and thus provided the highest confidence. Both couloirs 112 and 125 had the lowest measured snow on April 12th and the most snow on March 31st and March 7th.

Both couloirs 112 and 115 had cornices that resulted from snow loading due to blowing snow. The RPAS data were helpful in mapping cornice height and shape. However, the RPAS never flies during storms, which is often when avalanches occur. Instead, it is flown between storms. With wind the leading cause of avalanches, we explored whether the ARWIS data, particularly the snow height at the ARWIS site, during wind, and blowing snow, could provide insight into the dynamics of the snow surface in the couloirs between subsequent RPAS surveys.

3.3. ARWIS Data Overview

Wind transporting snow into couloirs is the prominent cause of avalanches in Atigun Pass. Therefore, we explored wind, as measured by the ARWIS. The most representative wind speeds and directions on the south side of Atigun Pass were measured by the ARWIS, depicted in Figure 3.11.

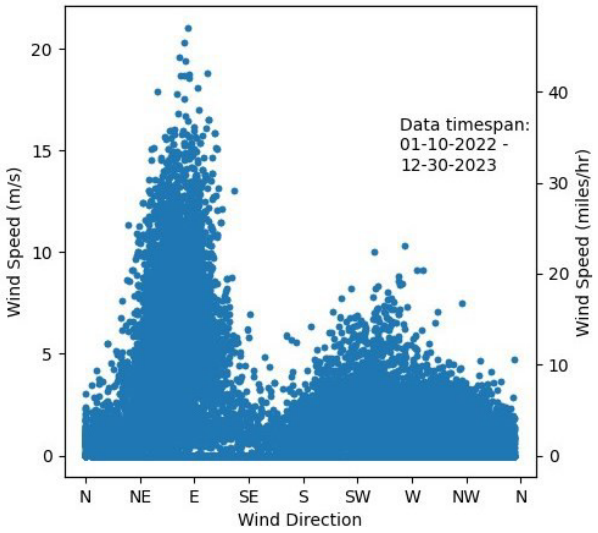

Figure 3.11. A year-long collection of wind speeds and directions at the ARWIS station.

Figure 3.11 depicts a year's worth of wind data at the ARWIS site, showing two prominent peaks at E-NE and W-SW. Winds higher than 7 m/s (15 mph) originated from the pass in the E-NE direction. The higher wind speeds from the E-NE were aligned with the snow loading on the windward east side of couloirs 112 and 115. Generally, winds above 5 m/s are required to transport snow. Winds originating from the SW are generally associated with a system in the region and possible precipitation. The broader peak of winds from the SW occur because the winds come from the bottom of the valley, which has a broader opening than the NE winds coming through the narrow pass. We found a seasonal pattern of the S winds converging toward the NW by winter peak and returning to the S by summer (not seen).

Blowing snow flux is generally a function of wind speed. This is nicely seen in Figure 3.12. The upper panel depicts measured wind speed, and the lower panel shows wind direction on the left (red) and blowing snow (black) on the right.

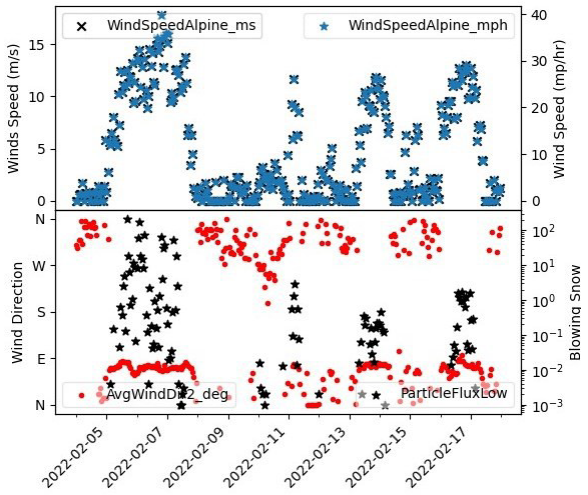

Figure 3.12. Upper panel: Measured wind speed in meters per second and miles per hour. Bottom panel: Measured wind direction on the left (red), and the measured blowing snow (in black) on the right.

The blowing snow is noticeable when the measured wind was above 5 meters/second. The units of the blowing snow are g/m^2/s. However, because we were still evaluating the accuracy of blowing snow measurements, we focused on the relative magnitude changes. Figures 3.11 and 3.12 support the understanding that winds of higher than 5 m/s are responsible for most blowing snow events on the south side of Atigun Pass.

3.4. Linking RPAS Data Products with ARWIS Data

Blowing snow, wind speed, and snow height data from AWRIS between January 10th and April 15th are depicted in Figure 3.13. This is the period when the bulk of the RPAS surveys were conducted.

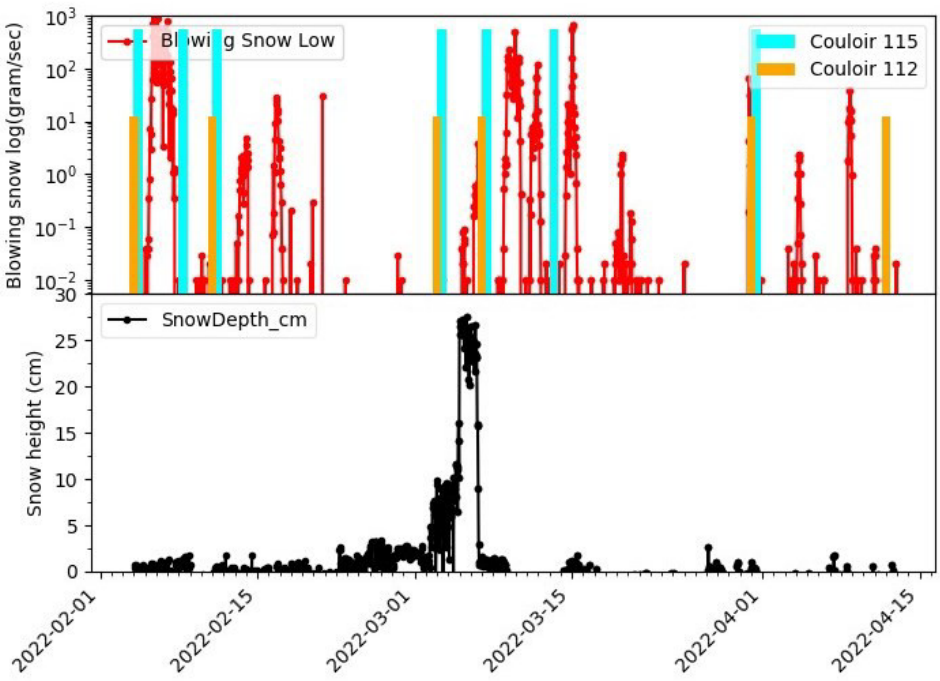

Figure 3.13. Upper panel: measured blowing snow (in red) and the RPAS survey dates (in cyan and orange) over the studied season. Bottom panel: The ARWIS measure of snow height during the respective study period.

To link the RPAS survey—mainly conducted between storms—with the activity during storms that shaped the surface during storms, we explored the correlation of blowing snow events and measurable snow surface height changes in couloirs 112 and 115. Figure 3.13 depicts wind speed and blowing snow on the upper panel and snow height on the lower one. The cyan and orange lines mark RPAS survey dates. Of the entire period from January 10th to May 1st, only for a few days—March 3rd-6th—did the ARWIS record significant snow of 10-25 cm. Apart from this episode, the rest of the period had less than 2.5 cm of measurable snow. In fact, the 25 cm of snow eroded within a few hours on March 6th; also see Figure 3.14. An inspection of the snow flux values on the upper panel, the flux magnitude and extent on March 9th through 10th and 11th, shows that more snow was transported while the ARWIS measured no significant amount of snow on the ridge. Thus, to some extent, significant amounts of snow (>2.5 cm) on the ridge were unnecessary for large blowing snow events.

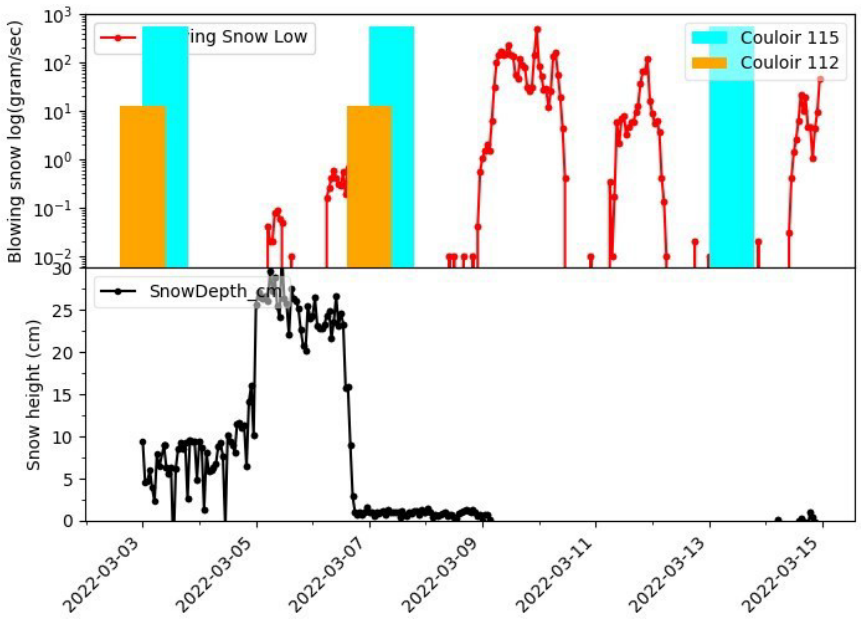

Figure 3.14. A close look at the changes in early March. Upper panel: Measured blowing snow (in red) and the RPAS survey dates (in cyan and orange) over the studied season. Bottom panel: The ARWIS measure of snow height during the respective study period.

The two most significant blowing snow events that were also captured by the RPAS before and after were the events between February 5th-8th and March 8th-12th. The more minor blowing snow event on March 6th eroded the snow from the ARWIS site from about 25 cm down to about 2 cm. The two sizeable blowing snow events shared similar durations and comparable blowing snow values. Therefore, we used the RPAS surveys to evaluate the impacts of the two large and one small blowing snow events.

We next used the RPAS surveys to evaluate how much the snow surface height changed over the respective periods. We used the cross-sections identified earlier for this analysis. Because the ARWIS-measured changes in snow height were in the tens of centimeters and less, analysis of these changes with the RPAS DEMs was at the edge of the location accuracy confidence.

Of all the couloirs surveyed by the RPAS, couloir 115 was surveyed most frequently. With couloir 115 downwind from the ARWIS, we expected to have the highest detail and correlation with the ARWIS data. We used these data to analyze changes in the snow height first. We developed Figure 3.15 for this analysis.

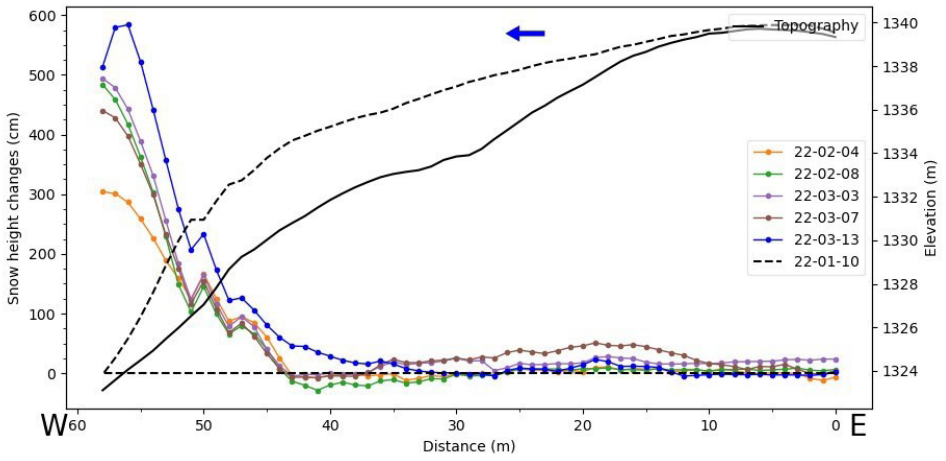

Figure 3.15. Couloir 115 surface-height changes based on the first RPAS survey, 2022-01-10. The solid line is the topographic cross-section, and the dashed lines are the cross-sections of the RPAS surveys.

In Figure 3.15, the topographic profile is depicted by the thick dark line, with the elevation profile on the right axis. The cross-section of the snow surface, as measured by the RPAS on January 10th, is depicted above the topography as a dashed line. The same cross-section black line from January 10th is also depicted with the value of zero. This first survey is a reference for the following cross-section surveys. The plot using the left y-axis depicts changes in the snow height with respect to the surface on January 10th. For example, one can notice that at the right side of the figure (on the exposed side of the ridge where the AWRIS was located), the snow was the highest on March 3rd. The AWRIS snow height data (Figures 3.13 and 3.14) peaked by an additional 15 cm on March 5th, and snow was mainly eroded by March 7th (brown line) during 10 m/s winds. The eroded snow from the ridge drifted downwind and accumulated on the leeward, 10-35 meters away, as shown by the brown line standing out. In fact, two small avalanches occurred in this couloir by March 7th. Following much stronger winds of 15 m/s, strong winds between March 9th and12th eroded the leftover snow on the ridge and transported and fed the cornice, about 55 meters, until it reached its largest size (Figure 3.16), a dark-blue line, by March 13th.

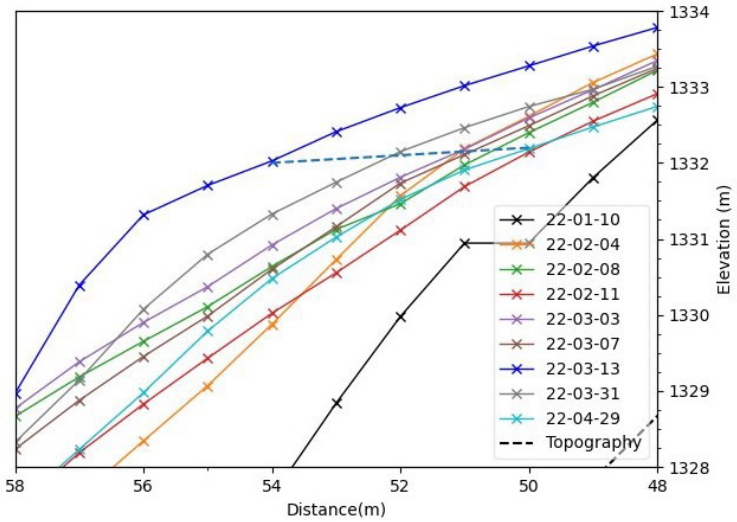

Figure 3.16. Couloir 115 cornice cross-sections. The dashed line depicts the cornice advancement over the study period.

Similar blowing snow magnitudes and durations were measured on February 4th-8th and captured by our data. However, that snow does not seem to have resulted in measurable cornice growth. The data did show a dramatic gain of more than 1.5-2 meters of snow just past the cornice, as seen in Figure 3.17. But this area of significant snow height increase was also where we saw the lack of distinct features (figures 3.2,3.3, and 3.4) and thus should be viewed with considerable skepticism.

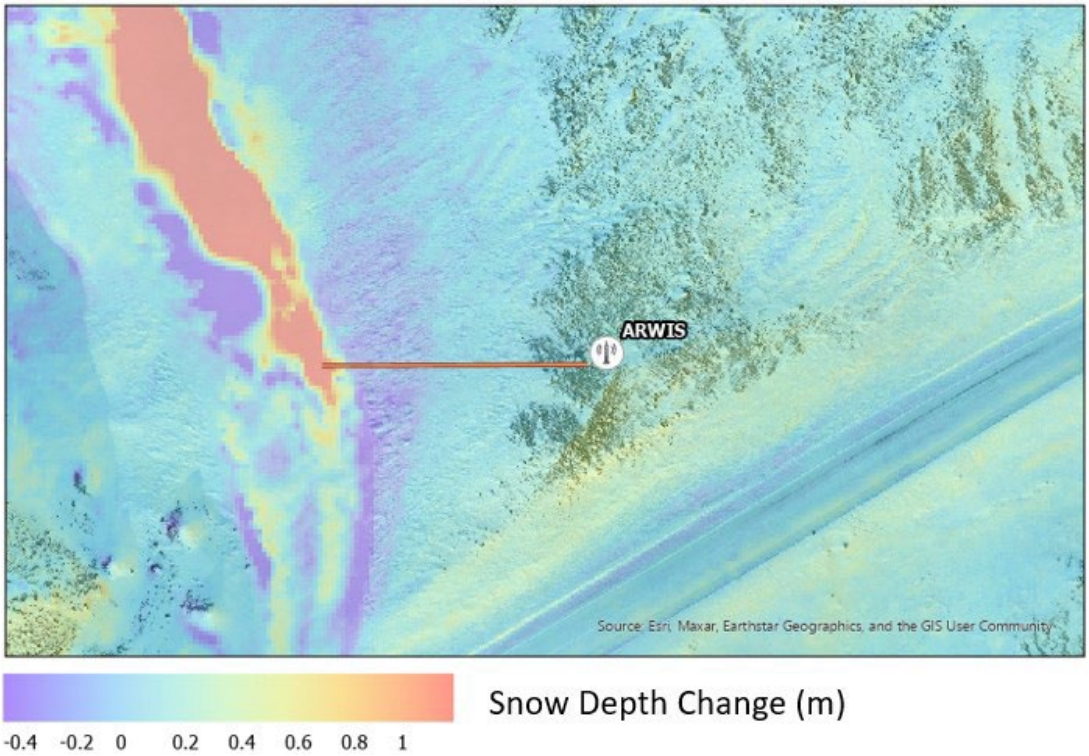

Figure 3.17. Couloir 115 dDEM of February 8th–4th with the orthomosaic from February 8th as a background.

Figure 3.18 depicts the changes in snow height between March 3rd and 7th. Following new fresh snow, winds of about 10 m/s consistently stripped the fresh snow off the exposed ridges.

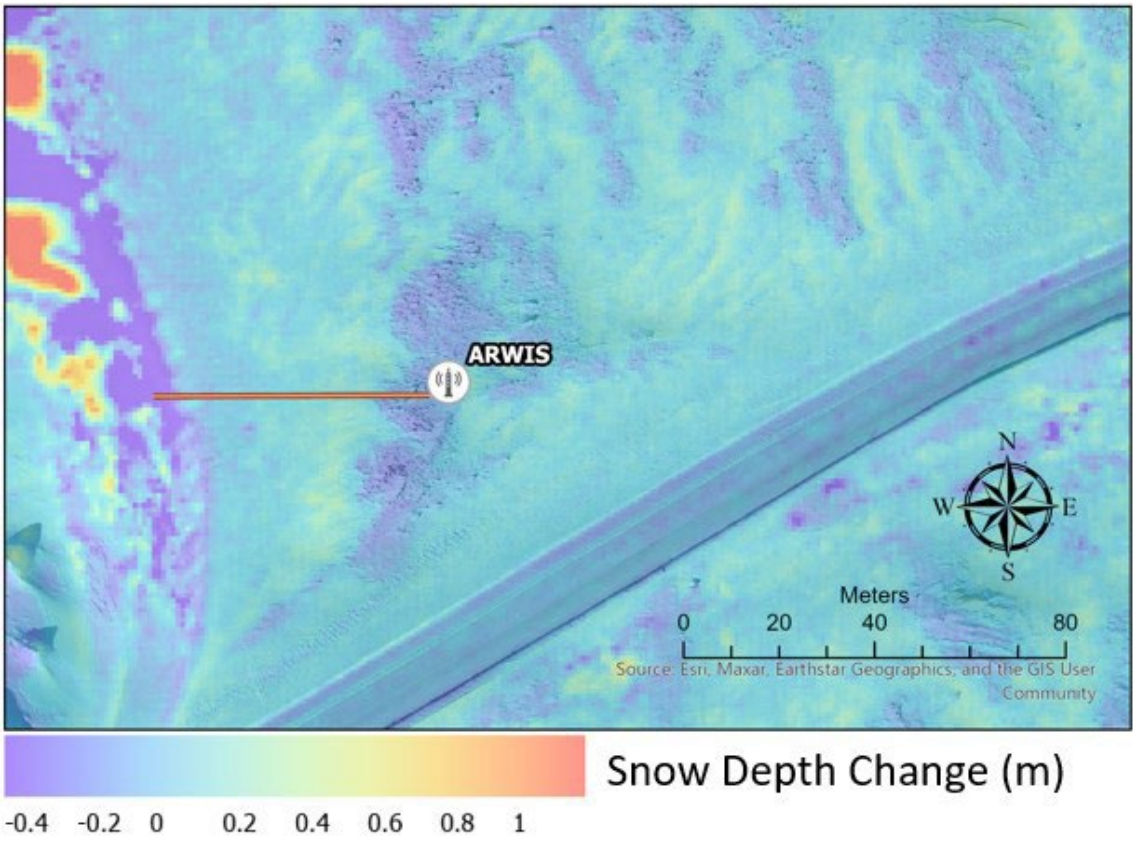

Figure 3.18. Couloir 115 dDEM of March 7th and 3rd.

Following the wind event that stripped snow off the top of the ridges was the more significant wind event (March 7th and the 13th), and the impacts are seen in Figure 3.19. Strong winds, about 15 m/s, relocated snow from the road corridor and below the top of the ridges, contributing to the most significant measurable cornice gain during the study.

Figure 3.19 depicts virtually no change (light-blue) in the snow height at the ridge, which was stripped in the previous, weaker wind event.

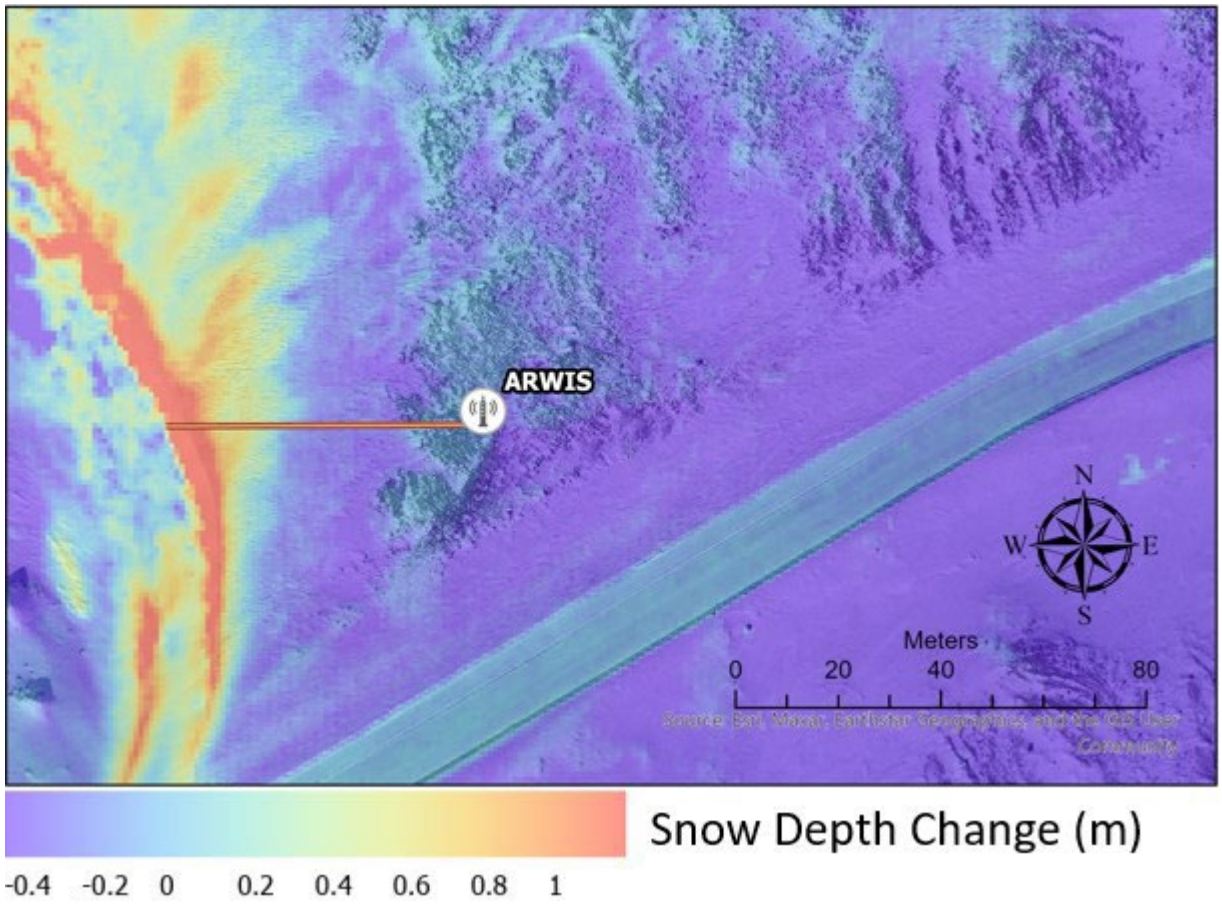

Figure 3.19. Couloir 115 dDEM of March 13th and March 7th.

Figure 3.19 depicts a significant loss of snow along the road corridor and little to no change along the ridges. This difference in snow height during the significant blowing snow event (March 8th-13th) suggests that little available snow on the hillsides could be a source of snow for significant wind events, even when the ridges are mostly stripped of snow. This central conclusion can help us understand snow-transport potential before an avalanche.

We next evaluated the snow height dynamics at couloir 112, which often avalanches on the Dalton Highway below. Couloir 112 is downwind from couloir 115. For this analysis, we used a cross-section of the upper part of the couloir, as seen in Figure 3.9. This cross-section sampled a cornice that often plays a role in the couloir avalanching. This is caused either by the collapse of the cornice or by critical snow loading below it. The prevailing winds from Atigun Pass are down the valley (east-west); however, examination of snow erosion features above the cornice cross-section indicated a north-south wind. This was concluded from the exposed rocks pointing north and the snow tail pointing south. The cross-section about 20 meters around the

cornice, with about 10 meters above and below it. Figure 3.20 depicts the changes in the snow height surface. To aid in interpreting the figure, the x-axis is labeled with “N” and “S” for north and south, respectively. The right side, y-axis, of the figure, depicts the topographic elevation profile (thick black line), and the snow height surface as of February 4th is depicted as a black dashed line. The February 4th black dashed line is also the reference line at 0 (cm) on the left y-axis. All other cross-section profiles are measured with respect (difference) to the snow surface as of February 4th.

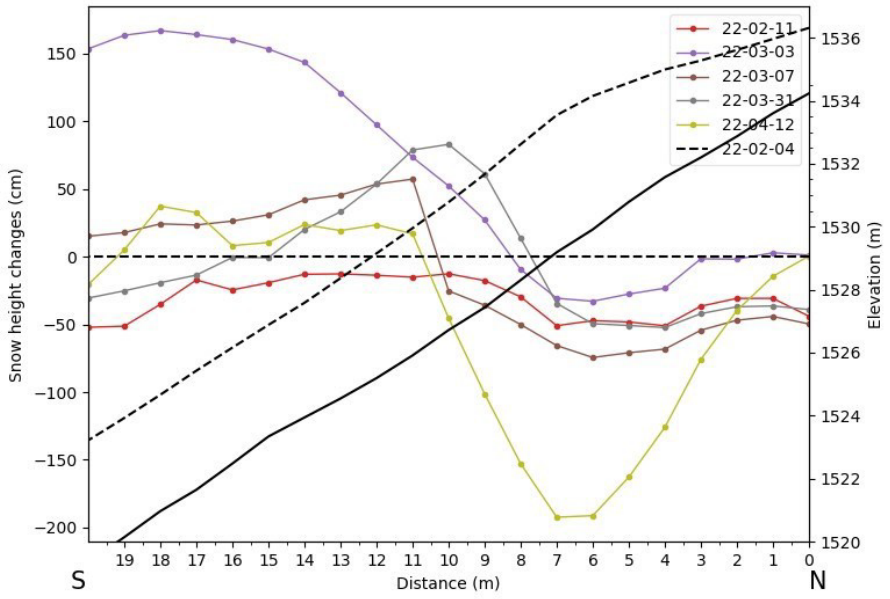

Figure 3.20. Couloir 112 surface-height changes from the first RPAS survey, 2022-02-04. The solid line is the topographic cross-section, and the dashed lines are the cross-sections of the RPAS surveys.

Without background information, it would be almost impossible to tease out the cornice locations in the plot. The 2D raster, as well as sampling at 1 meter, blurs the steep stepwise elevation change. On February 11th, the cornice is about 6 meters from the plot origin and advances by March 31st to about 10 meters.

In both cases, there was a slight drop in height past the maximum—which is barely noticeable. Figure 3.21 magnifies the cornice cross-section and highlights the cornice advancement over the study period, with a dashed blue line highlighting this difference. Figure 3.21 shows that following the large wind event between February 4th and February 8th, measurable snow erosion of 25-50 cm occurred along the cross-section. The loss was much

smaller past the cornice and more significant at the end of the cross-section. With snow seen in AWRIS data by March 3rd, the March 3rd cross-section (purple) gained about 25 cm of snow upwind of the previous cornice location. After that, there was a substantial increase of more than 150 cm. This could indicate a small avalanche before or after the new snow. The March 7th survey followed a wind event of about 10 m/s that stripped the fresh snow from the ridges. In this cross-section, the survey is indicated by the brown dashed line. The cross-section depicts a drop of about 50 cm, from the beginning of the cross-section until the 8-meters mark. From 12 meters on, the snow loss increased substantially, perhaps indicating a small cornice collapse. In fact, the orthomosaic from March 7th and the differential DEM (dDEM) (Figure 3.22) depict a small avalanche farther down the valley—the collapse of a different section of the cornice. By March 31st, the cornice was noticeably farther away, at about 11 meters. This was consistent with the significant wind and blowing snow event between March 8th-12th. Because the RPAS surveyed couloir 115 on March 13th, but skipped couloir 112, we think the cornice growth was due to the winds and blowing snow of March 8th-12th. Then, by April 12th, a noticeable large cavity appeared, centered at about 6 meters, a significant collapse of the cornice after two months of mostly growth! However, the collapse of the cornice did not seem to have triggered a noticeable avalanche.

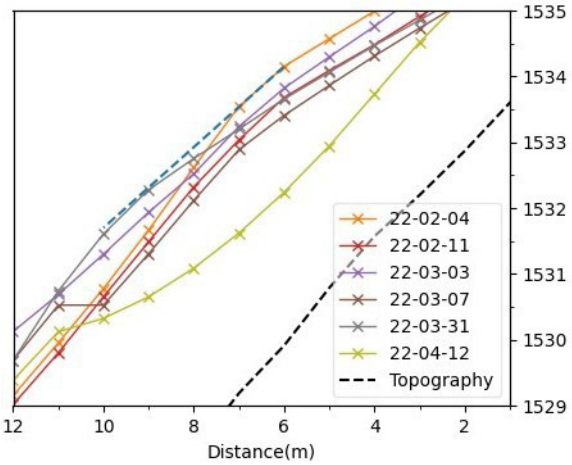

Figure 3.21. Couloir 112, close view of the cornice area surface-height cross-section. The dashed blue line depicts the cornice advancement over the study period.

The spatial context that dDEMs provide can spatially extend our understanding from looking only at the cross-section plots. Figure 3.22 depicts the impacts of the two large wind events: February 4th 11th and March 8th-12th on couloir 112. On couloir 115, only the second

event resulted in a noticeable increase in the cornice size. This seems to have played out similarly on couloir 112. We see that the cornice grew substantially during the second wind event. We also see a small avalanche (bound in a black line) that started near the cornice and then slid to about 200 meters from the road. The upper part of the avalanche is shown as a snow loss (negative values) in purple, and then where the bulk of that avalanche stopped is depicted in red and the end in yellow (positive values).

Figure 3.22. Couloir 112 dDEM. Left: The dDEM of February 11th - February 4th,bound by a black line. Right: the dDEM of March 31st -7th, depicting the large cornice growth at the top.

Figure 3.23 on the left depicts changes in the snow height between March 3rd and March 7th (following the 10 m/s winds). During that event, there was a small avalanche near the bottom of the couloir, highlighted in black. On the right of the figure is the respective orthomosaic capturing the avalanche aftermath.

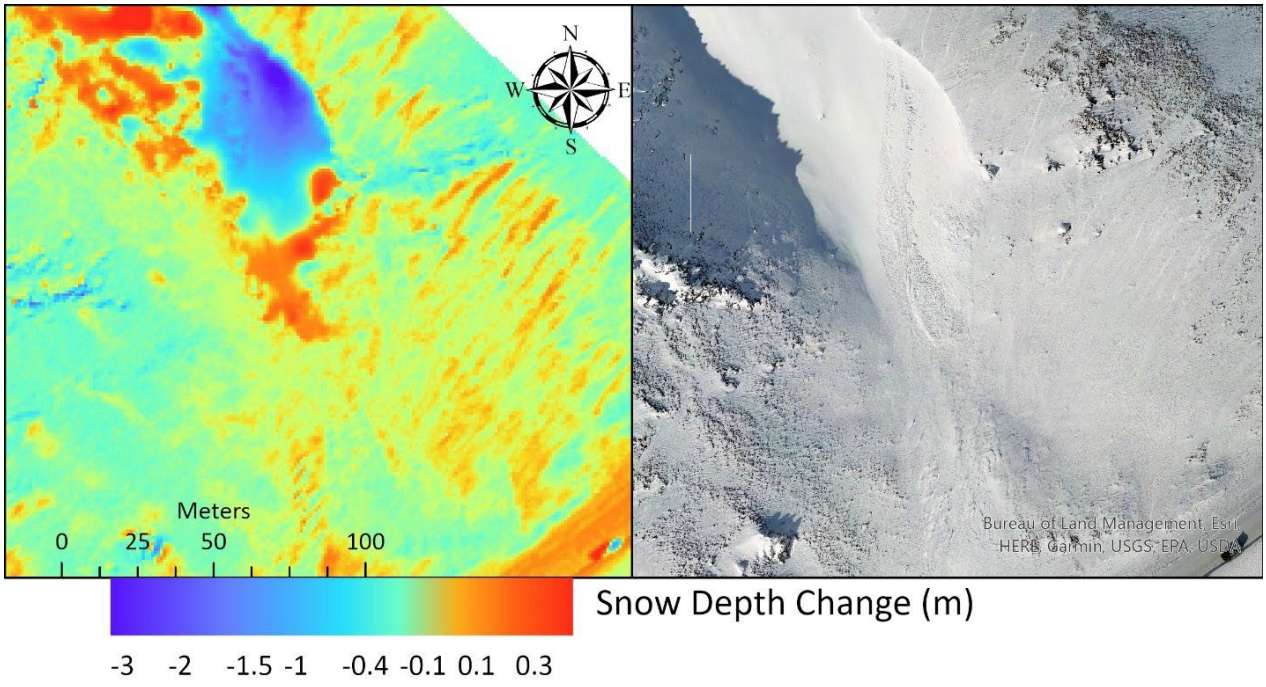

Figure 3.23. Couloir 112 dDEM March 7th – March 3rd. A small avalanche, bound by a black line, is seen in the lower center of the figure.

During the seasons of RPAS data collection, no large avalanches came close to or covered the road on the south side of Atigun Pass. Therefore, we only see small ones. However,

this also means that if small avalanches are captured well, then, indeed, larger ones would also be captured. The major steps in the cornice growth and collapse cycle are seen in figures 3.24 and 3.25. In Figure 3.24on the left, we see the narrow arc of red showing the significant cornice growth depicted by those pixels. On the right is the respective orthomosaic depicting the sharp cornice edge. Also seen is the avalanche control effort, consisting of two artillery rounds used to assess the stability of the cornice at two different spots.

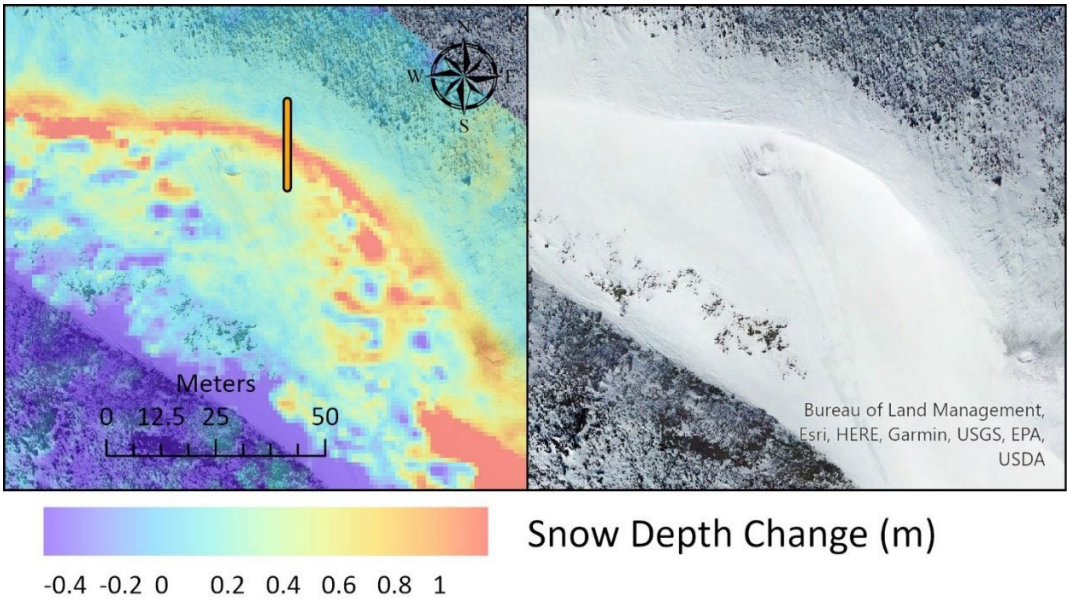

Figure 3.24. Couloir 112 dDEM March 31st – March 7th. This dDEM depicts the most significant cornice growth seen in the RPAS surveys during the study period.

Knowing where the cornice was last seen in Figure 3.24 helps us understand where it collapsed. The collapse was captured by examining the difference in snow height between March 31st' and April 12th. At this exact location, we see in Figure 3.25 the spatial extent of the collapse in purple and blue. The orthomosaic on the right is missing the distinct edge of the cornice seen in Figure 3.24. Vague remnants of the artillery shot provide a sense of orientation.

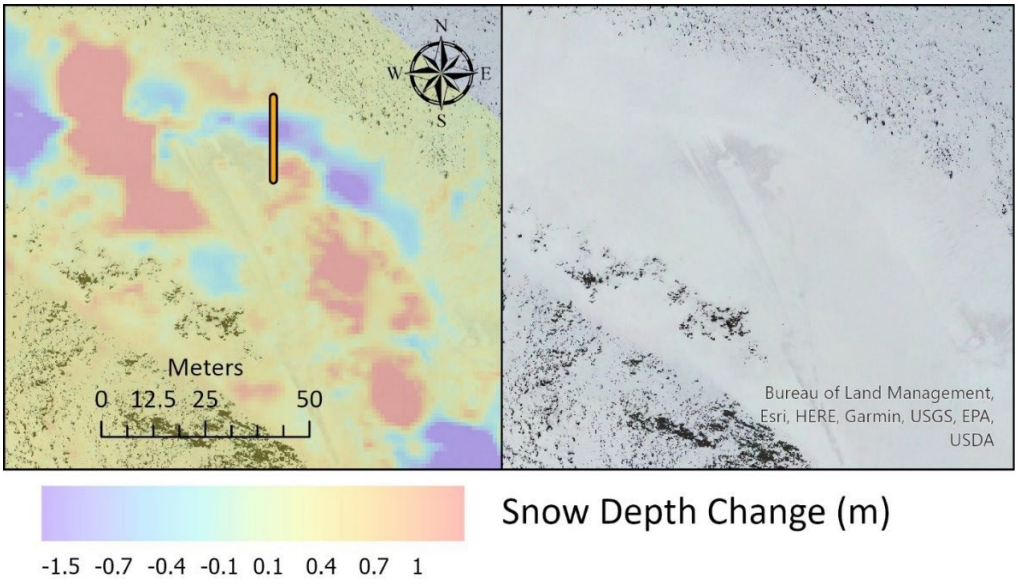

Figure 3.25. Couloir 112 after a cornice collapse. Left: The dDEM of April 12th - March 31st. A black line binds the collapse of the cornice. Right: the orthomosaic of the cornice collapse aftermath.

The two large blowing snow events on February 5th-7th and 9th-12th had similar blowing snow values but led to different consequences. The event in February produced little change in the snow on the ridges and did not increase the cornice growth by meaningful size in both couloirs 115 and 112. The event in March did produce cornice growth to their most significant values of the season in both couloirs 115 and 112. Therefore, it seems that cornice growth at couloir 115 could at least be analogous to that at couloir 112.

We looked carefully at wind speeds, wind direction, blowing snow values, and temperature. While the February event seems to have had more sizeable blowing snow values by a bit, it seems the largest difference was the temperature. The February event started at -24C, with the temperature dropping all the way to -35 C by February 7th at noon. On the other hand, the coldest temperature during the March event was warmer than -24C, with most of the snow blowing snow during a temperature closer to -16C. Thus, temperature can be considered a major factor in a cornice growth or snow loading below it during similar blowing snow conditions.

3.5. Linking ARWIS Measured Blowing Snow Data with M&O Highway Reports

ADOT&PF has no records of avalanches during February-May 2022, when the bulk of the RPAS surveys were conducted. However, during the fall of 2023, there was quite a bit of avalanche activity, which enabled us to compare wind and large blowing snow events with

ADOT&PF-reported avalanche events. Figure 3.26 depicts wind speed in the upper panel and blowing snow on the lower left. On the lower right of the panel are the couloir numbers (112 and 125 were spatially analyzed earlier). Natural and controlled avalanches are depicted by green and red circles, respectively. In the figure, there are three groups of avalanches (natural and induced): October 20th, November 16th-18th, and December 11th-12th. Four avalanches occurred on December 11th within 6 hours of 15 m/s or 30+ mph winds and significant blowing snow, which shows the important influence that wind and blowing snow have on inducing avalanches.

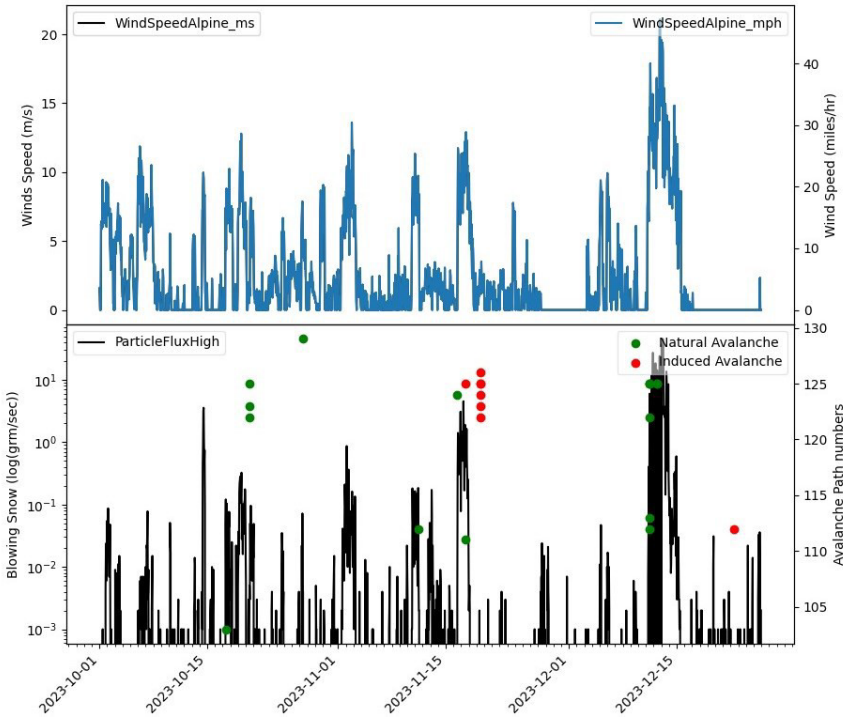

Figure 3.26. Upper panel: Measured wind speed. Lower panel: Measured blowing snow values in black with documented avalanche occurrences by ADOT&PF on the right. In green are natural avalanche occurrences, whereas in red are ones induced by artillery fire.

The measured blowing snow data by the ARWIS correlated nicely with M&O's reported drifted snow. Figure 3.27, in both panels, compares the blowing snow measured by the ARWIS on the left axis with different drifting and blowing snow conditions as reported by the M&O staff on the right axis.

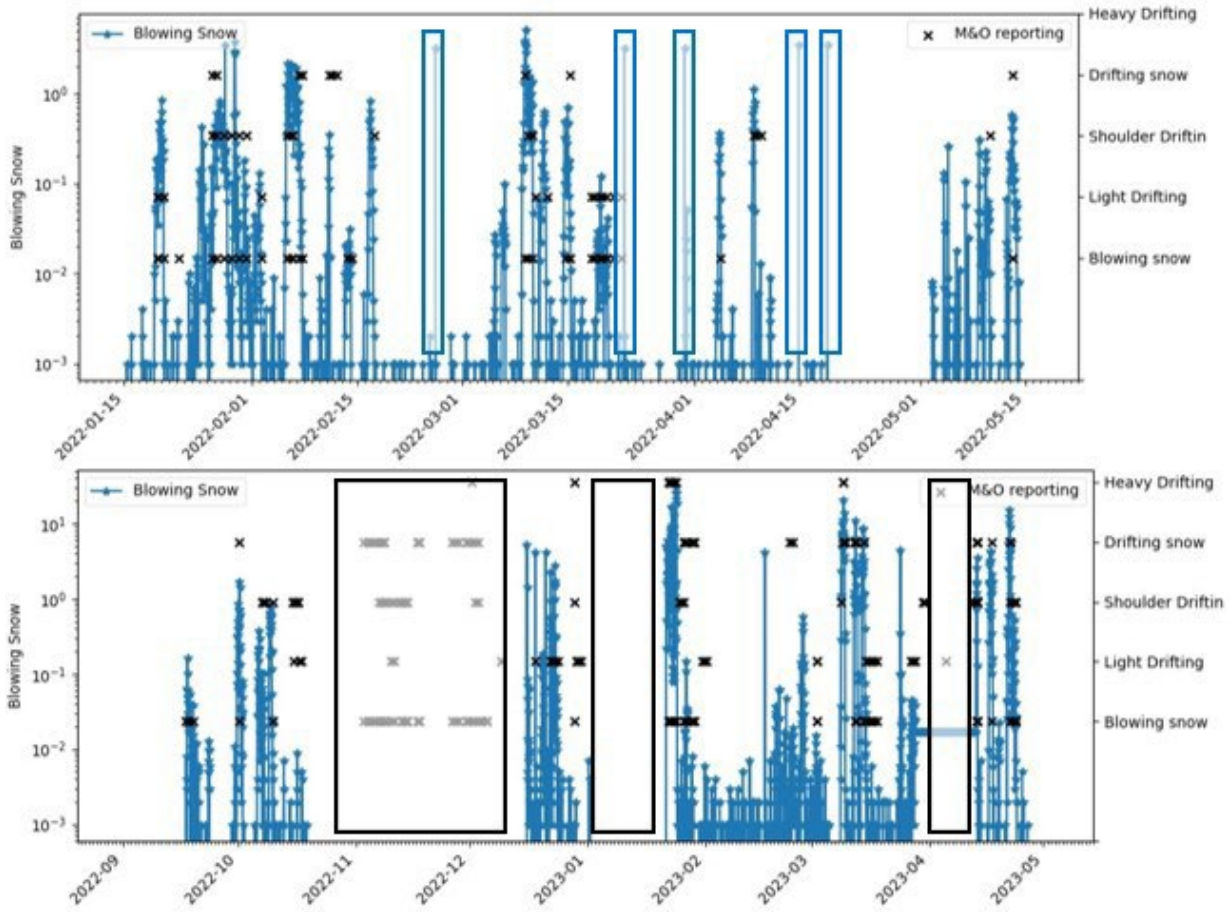

Figure 3.27. Comparing ARWIS blowing snow measurements with ADOT&PF-reported drifting and blowing snow conditions.

Without the black rectangles that show periods when the blowing snow was not producing meaningful data (probably because of heavy rime), and some possible outliers (blue rectangles), there seemed to be good agreement between the reported drifting and blowing snow conditions and the measured blowing snow event (timing), and the magnitude of the peak correlated somewhat with the drifting intensity. However, the M&O reporting was far from accurate, and therefore, there was no perfect fit. The reports covered a large stretch of the Dalton Highway; mileposts 235-245 span over 14 kilometers (direct line), including both the Chandalar Shelf and about 2 kilometers (one milepost) on the north side of Atigun Pass. This stretch of road spans three very different geographies that experience different precipitation, wind, and blowing and drifting conditions. Therefore, reporting of drifting snow at the Chandalar Shelf on the north side of the pass may not coincide with measurable blowing snow on the south side. Also, the definitions of different reported drifting classes are not clear, and the differences between them

seem vague. In addition, there are two shifts and different staff reporting on road conditions. Together, all of this resulted in inconsistencies. We did try to find a correlation between the blowing snow ten hours before the reporting of some drifting but did not find an obvious correlation with reported snow drifts.

Chapter 4 DISCUSSION

4.1. Operating an RPAS to Map Snow in the Arctic and Mountains

During the project, the avalanche practitioner completed more than 24 surveys of key avalanche-prone couloirs. However, during this time there were no avalanches on the south side of Atigun Pass to capture. We made progress in removing barriers to create smoother RPAS operations, but there are still significant barriers, such as the aircraft of choice, the DJI Phantom 4 RTK. A hard-wired altitude restriction mechanism in the aircraft prevents it from reaching sufficient altitude and full coverage of the couloir, specifically at the start zone where it matters most. This limitation makes operation of the aircraft reliant on manual operation, instead of operators being able to rely on autopilot for the entire flight. The actual flight is generally short. What takes the most time is the aircraft and RTK setup; the actual flying is about 20 minutes.

The winter arctic environment is harsh because of sustained bitter cold temperatures, wind, and low light or darkness. For the most part, the temperatures did not restrict operations. By keeping the aircraft batteries in a warm truck before operation, we were able to fly in temperatures that were at least as cold as -30C if not colder. Of the three couloirs, 112 and 115 were completed on a single battery, and only 125 required two batteries. Of course, an aircraft with longer endurance could survey several nearby couloirs in a single flight, which could save on setup time.

The RPAS can fly in strong winds of <10-12 m/s, but such winds induce blowing snow and affect visibility of the aircraft and the visibility of the camera capturing the surface. Therefore, these winds are not conducive to robust, high-quality mapping. We conclude that the wind limitation is more due to the object being mapped than to the RPAS's flying restrictions.

Light and its interaction with the snow surface create distinct features that are known as tie points. A high-density number of tie points is critical for the photogrammetry process. It was apparent in our data that surface brightness and roughness varied within a scene (from shadows) and across scenes (from time of year and low sun angle). More than a month of polar nights in Atigun Pass is a long time of insufficient light for a camera on an RPAS to detect surface features. Valleys between tall mountains and the north side of the pass are partly or entirely in the shadows before and after the polar night season. The shadows result in a low number of or no tie

points. Our survey data also included bright light conditions that had a low density of tie points or none. In this case, the low number was due to smooth snow surface with few to no identifiable features for the naked eye and the camera. In our data, there were generally two scenarios for featureless snow: 1) fresh snow, such as on March 3rd and April 12th, and 2) the snow in the couloirs was not subject to high enough winds. Ridges on both sides of the couloirs prevent strong winds from transporting snow in a way that generates snow bed features. In addition, the strong wind that blows snow into the gully results in a smooth surface that, in some circumstances, perfectly matches the ridge. The problem was that our interest was to map snow height in the couloir to determine avalanche precursor conditions, and smooth snow hindered us from creating an accurate representation of the snow surface. The general low snow on the ridges, and relatively small changes in snow height, meant that we were analyzing a relatively weak signal and high noise environment.

Lee et al. (2021) did a rigorous study on the factors that influence the accuracy of mapping shallow snow depth (20-30 cm) using photogrammetry. They found a correlation between the number of tie points and survey product accuracy: the higher the tie-point density the higher the product accuracy and vice versa. They also discovered that in fresh snow there are few to no tie points, which results in significant error or even fully inhibits the photogrammetry process. They also hypothesized that shadows on the snow, such as when the sun is low, in the morning, and later afternoon (9:00 am and 3:00 pm), degrade photogrammetry product accuracy. They found a strong spatial correlation between shadow location and increased snow-depth error. Snow depth was significantly higher in the shadowed areas. A large dynamic range of high brightness and shadows in the morning and evening caused bias in the overall photogrammetry results.

The low density of tie points on a smooth snow surface, and the erroneous data that shadows produce, motivated Buhler et al. (2017) to explore the use of the near-infrared (NIR) spectrum when using photogrammetry to map snow. They found that augmenting the generic green and blue channels with an NIR band improved snow map accuracy and significantly improved the map accuracy when only the NIR band was used. In the presence of shadows, the NIR band outperformed the visible spectrum channels, with the latter resulting in noisy areas with errors as high as 10 meters and large cavities in the data. The NIR channel responded better to bright and shadowed snow and provided better contrast over a smooth snow surface because of

the variability of snow grain size. Adams et al. (2018) compared the data from an RPAS with a camera with the NIR spectrum and a terrestrial light detection and ranging (LiDAR) scanner (TLS). Their camera setup using the visible spectrum reached DSM accuracies of better than 29 cm in well illuminated conditions; however, under shadows, the accuracies of the DSMs and SDMs (snow depth maps) were 49 and 47 cm, respectively. Meanwhile, the NIR setup performed much better at 0.19 and 0.23 cm, respectively. Maier et al. (2022) used a multispectral camera and photogrammetry to map snow depth. The authors used the red channel components (red, red-edge, and Near IR), 600-860 nm, and evaluated them by using a principal component analysis (PCA). The red channels had the highest correlation with the first PCA, and the first PCA represented more than 70 percent of the data. With such promising results from use of the NIR spectrum and the fact that it is easily attainable by removing the NIR filter from any standard camera, it seems to be a promising avenue of research toward producing robust, high-accuracy snow-height maps using photogrammetry.

4.2. ARWIS Data Complementing RPAS Surveys

The ARWIS's ability to measure wind speed and snow transport provides insight into in situ conditions that lead to avalanches and snowdrifts on the south side of Atigun Pass. Figures 3.26 and 3.27 both depict a satisfactory correlation between the recorded blowing snow and reported drifting and blowing snow. At this stage of the research, the correlation is more qualitative and less quantitative. There are only a few dozen known avalanches in our database, and that is too few to infer the necessary wind conditions or the amount of transport snow that will significantly increase avalanche likelihood. However, an entire season of avalanche data might bring us much closer to being able to infer avalanche precursor conditions from the ARWIS data. To increase the reliability of the avalanche activity database, there might be value in utilizing satellite products to detect and quantify avalanche size. The remote location of Atigun Pass, with long periods of dark and blowing snow or whiteout conditions, makes it difficult to identify and document avalanche activity. Satellites that use synthetic aperture radar (SAR) cover significant ground, can measure the landscape through inclement weather, and are independent of the sun's illumination. For example, Bianchi et al. (2020) demonstrated an impressive 66 percent success in detecting avalanches with Sentinel-1 SAR data and a trained neural network. This is one example, and we think there will be more options in the future. We believe that with better avalanche activity documentation, such as from satellite imagery, we will be better able to

correlate avalanche activity and avalanche precursors, such as wind and snow transport magnitude, and in the future generate reliable warnings.

4.3. Cornice Evolution and Blowing Snow and Wind

The value ability to measure snow transport quantity and to map the snow height nearby downwind offers important insight into spatial-temporal snow-transport activity and its role in inducing avalanches in Atigun Pass. Couloirs are excellent snow-transport traps. Therefore, we expected there to be a direct correlation between measured snow-flux and accumulated snow in the couloir. However, poor texture in the couloirs renders the photogrammetry products unreliable for quantitative analysis. We therefore focused our analysis on surfaces that are exposed to strong winds, such as ridges and cornices. The collapse of a cornice has the potential to initiate an avalanche, and larger cornice collapses are associated with larger avalanches. Therefore, we focused our analysis on cornice size evolution and the transport-snow that feeds its growth. The ARWIS records wind and transport snow flux. Three events during our study of winds and blowing snow drew our attention. The three events occurred on February 5th-7th, March 6th, and March 8th-12th, labeled as events I, II, and III respectively. These events depicted the most significant changes in snow height. Event II was about six hours long, with a recorded wind speed of about 8-10 m/s that eroded ~25 cm of fresh snow at the ridge tops. Below the ridge tops, winds were sufficiently weaker and did not alter the snowpack. Events I and III depicted the most significant transport snow events, with recorded wind speeds of about 12-14 m/s, generally with similar directions (NE-E), and ample snow flux. However, among the three events, only the third one resulted in significant cornice growth, of about 1 meter, in both couloirs 115 and 112. What conditions hindered and were conducive to cornice growth in events I and III, respectively?

Literature documenting cornice accretion is limited, and in general it only depicts mild temperatures in comparison to our study site in Atigun Pass. The studies often occurred in the Alps, Svalbard, and wind tunnels. Of the three events of interest, the recorded temperatures were -35C, -15C and -22C for Events I, II, and III, respectively. Event III experienced significant (~1-m) cornice growth, and Event I experienced no growth. Vogel et al. (2012) reported on the meteorological control of cornice dynamics in Svalbard. Of N=26 recorded accretion events, the median was about -6C, and the Q1 and Q3 quartiles were -15C and -2C, respectively. Q_0 was at about -22.5C. An N=579 of no accretion days had a Q_1 slightly warmer (~-13C) and a Q_0 of -30C.

Kobayashi and Ishikawa (1987) reported cornice growth at air temperatures as cold as -8C. Naito and Kobayashi (1986) recorded cornice accretion as cold as -20C. Event III was close by a few degrees to other reported cornice accretion events. Event I was consistent with Vogel et al.'s (2012) observations of no reported cornice accretion at temperatures colder than -22.5C. Se et al. (2023) showed that liquid water content (LWC) correlated with sticking efficiency, an essential process in cornice accretion. Thus, at very cold temperatures (-30s C), low LWC conditions could explain why we do not observe cornice accretion. Sublimation might also play a significant role and prevent snow from adhering to the cornice.

Winds have generally proved to play the most significant role in cornice accretion. There have been several reports of cornice accretion under various wind speeds. Naito and Kobayashi (1986) and Vogel et al. (2012) measured winds speed during cornice accretion, at 4-8 ms^{-1} and 12 ms^{-1}, respectively. Yu et al. (2023) evaluated cornice accretion conditions in a wind tunnel and found that cornices appeared only under moderate wind conditions, one to two times of the threshold speed, and that the cornice growth rate in length and thickness was favorably affected by the combination of snow deposition and erosion. The lower limit for cornice growth was approximately the threshold wind, and the upper limit was when the erosion rate was higher than the deposition rate. The cornices' length growth rate reached a maximum speed of approximately 40 percent higher than the threshold windspeed. Yu et al. (2023) concluded that the reported variability in suitable wind speed for cornice accretion stemmed from variability in the local roughness length and threshold wind speeds. It is essential to understand that cornice accretion is a slow process. During peak cornice growth-rate in Svalbard, Hancock et al. (2020) recorded accretion rates as 14-17 $mmhr^{-1}$. Thus, 1-meter of cornice growth during a single storm event at a rate of 15 $mmhr^{-1}$ would take about 66 hours! So even in the right wind conditions, cornice growth would take about three days.

Although cornice accretion efficiency decreases with increased wind speed, Yu et al. (2023) argued that wind speed should not be an indicator of cornice growth rate. The author stated that the combined effect of mass accumulation and erosion is the determining factor of cornice growth rates in length and thickness. The lower-end limit of wind speed is the threshold wind for snow transport, and the upper limit is when the deposition and erosion rates are balanced. Favorable deposition conditions are key for cornice growth. Filhol and Sturm (2015) argued that the spatial variability of snow surface properties (i.e., harness, geometry, grain size,

and layering) determines the effect that wind will have on snow: erosion versus deposition. Looking closely at the snow surface just a few meters upwind from the cornice formation at critical dates before and after events I and III shows the variability of surface properties and how they may indicate favorable or unfavorable cornice formation.

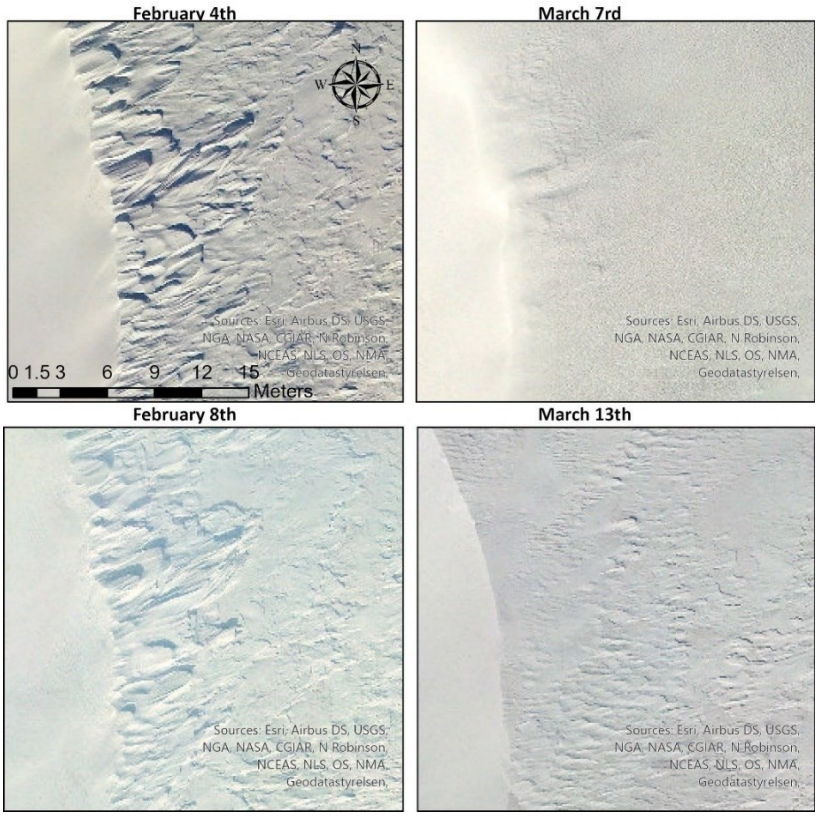

Figure 4.1. Views of the snow surface upwind from the cornice at couloir 115

Figure 4.1 depicts the snow surface at the beginning and end of events I and III. The snow surface on February 4th and March 7th before large wind and blowing snow events were vastly different. On February 4th the surface was heavily windblown and scarred in sastrugi, whereas on March 7th it was generally smooth of fresh snow that may have been lightly crusted at the surface by a short wind event on January 6th (Event II). The large wind and blowing snow values on February 4th seem to have barely changed the snow surface by February 8th. Whereas by March 13th, after similar winds and ample snow-transport flux, there was a large cornice growth, and barchans upwind from the cornice appeared. In essence, a cornice is a type of bedform and may fit a hypothetical evolution of snow bedforms, as stated by Filhol and Sturm (2015). They asserted that

(1) new snowfall provides material for transport
(2) there is sufficient wind (in the case of the cornice perpendicular to the ridge)
(3) there is the development of a field of barchan dunes (in our case the development of a cornice)
(4) over a period of time the snow surface of the cornice and upwind of it sinters
(5) when wind rises again, the next wind event erodes the barchan into a sastrugi, an erosion dominant environment, that does not favor cornice-accretion.

In our case of winds at -35C, with an extremely low LWC, it was an erosion dominated environment.

Van Herwijnen and Fierz (2014) reported that cornice formation generally happened during or soon after a snowfall; however, they did observe incidents of cornice growth in the absence of snowfall and the other way around. Naito and Kobayashi (1986) found that cornice growth requires suitable conditions of irregular dendritic-shaped snow grains. Yu et al. (2023) used dendrite and hollow column crystals in their wind-tunnel simulations. With the expected wind-blown grain to be round, this may play a key role in cornice accretion.

Another observation related to cornice accretion is that during Event III, we measured wind pumping for about 24 hours. During that period five apexes and troughs depicted wind variation of 12-14 ms-1. Bell (1993) argued that the penetration of wind into the snow is responsible for the formation of wind crust and tied the penetration of wind into the cornice with hard characteristics. Bell argued that wind-pumping significantly enhances snow metamorphism, which may help cornice accretion under cold temperatures such as those of Event III of -22.5C.

Multiple factors can contribute to or hinder cornice growth. Documenting cornice growth in the extreme cold temperatures that we studied, and the lack of literature to back up our observations, require us to increase our observations for more conclusive statements in the future.

Chapter 5 RECOMMENDATIONS

In this project, we proved that RPAS photogrammetry data processing can be streamlined into a completely hands-off routine. Also, we showed how the ARWIS data complements the more episodic RPAS surveys. We also found correlation between measured blowing snow data and reported avalanches and snow drifts on the Dalton Highway. We recommend continuing streamlining the RPAS and ARWIS data to achieve data assimilation, providing actionable information, and avoiding data saturation.

The in-depth analysis described earlier was one step further than what is currently available at the end of the APSIR data process. Providing the ADOT& PF M&O staff and leadership with graphical situation information can aid tactical and strategic resource allocation decisions. Integrating graphic analysis in ADOT&PF communications and reports can also improve their use and encourage better reporting of current drifting and avalanche conditions.

The current RPAS aircraft is limited by the altitude at which it can fly from its takeoff location. The bypass has been to temporarily fly the aircraft manually or to take off from a higher vantage point on the road. We recommend replacing the current RPAS with one that has no flight elevation restrictions. We recommend replacing the aircraft with one that can reliably execute the entire predetermined flight plan completely autonomously. We also recommend that the NIR filter in the camera on the aircraft be removed, which can lead to more accurate maps in areas that have shadows and snow of low texture.

Photogrammetry utilizes imagery from cameras that are ubiquitous on any commercial RPAS. A camera on the RPAS can provide high-resolution imagery, but poor lighting conditions, such as low light, shadows, and featureless surface, impede photogrammetry from being a reliable, operation-dependent solution for mapping snow in couloirs, where the surface is often smooth. The RPAS camera struggled to detect surface features in the gullies and hillsides where the snow was exceptionally smooth. Photogrammetry works impressively well in good lighting and with rich texture, but it struggles in their absence. The RPAS-photogrammetry is an excellent first-step solution when an RPAS mountain monitoring program is launched. Removing the NIR filter on the camera also has the potential to dramatically improve the current results. However, the limited availability of light in areas such as the Arctic hampers an RPAS system from becoming an operational asset for mapping avalanche precursor conditions. We

recommend that the RPAS at Atigun Pass be replaced with one with a LiDAR system. In that way it can be effective at mapping snow independent of lighting conditions and surface-texture conditions.

In comparison to the Alaska-south central regions that receive many meters of snow, Atigun Pass receives much less than that. Therefore, it is technically much harder to tease out smaller changes in snow height. However, the detection of small changes in cornice size is even more difficult with a 2D raster and a ground sampling distance (GSD) of 1 meter. Instead, we recommend transitioning to a finer spatial resolution (25 cm) and migrating from a 2D raster to a 3D point cloud. The 3D point cloud can better depict steep surfaces, vertical shapes, and cantilever shapes such as a cornice, and it would better at revealing critical small changes.

The ARWIS data highlighted environmental conditions on the south side of Atigun Pass that were not documented before. We saw how closely the wind and blowing snow correlated with snow drifting and avalanche occurrence. The ARWIS data provided context for the changes seen among RPAS surveys. However, this ARWIS site represented only the south side of the pass, and the north side was not monitored. Therefore, we recommend expanding the ARWIS network to include a site on the north side.

Both the ARWIS and RPAS data and systems exposed a weak IT infrastructure. Unreliable networks at the M&O camp inhibit access to outside resources. These resources include broader data access, computational power, and communication about the challenges of maintaining this stretch of road open to traffic. We recommend improving both Internet access and camp hardware to meet 21st-century solutions. Even heavy equipment is becoming more technological and will need better IT support soon.

The ARWIS and RPAS flights were limited in space and time. In the future, we would like to incorporate blowing snow and snowpack metamorphosis operational models to provide better spatial coverage and to help with avalanche risk assessment and decision-making.

M&O at the camps provides critical road and weather conditions information that could aid in calibrating the ARWIS to be sensitive to local environmental risks, whiteouts, avalanches, snowdrifts, and unexpected heatwaves. However, these reports are spatially located over large stretches of the highway and not a single MP. Also, the reporting is biased to the reporting M&O and is not objectively measured. We recommend training the M&O staff and adding references along the road to make reporting more uniform (for example defining “drifting” versus “heavy

drifting") and refining the reporting location to a particular milepost or a local M&O camp reference.

Chapter 6 CONCLUSIONS

The Alaska DOT&PF surveying group uses RPAS coupled with photogrammetry for its survey requirements. Airborne photogrammetry for measuring snowpack thickness has been well demonstrated in academic research and commercially. However, in both cases, the RPAS is flown and the photogrammetry data are processed by someone well versed in geospatial information system (GIS). In this project we made significant headway toward removing several manually intensive obstacles that will allow RPAS coupled with photogrammetry to be operational and therefore enable avalanche practitioners to focus on the impacts of newly available information.

We successfully launched an avalanche monitoring program based on RPAS and ARWIS at one of the most inhospitable and remote mountain highways passes on the North American continent. The avalanche forecaster has the difficult job of monitoring avalanche conditions in poor lighting, bitter cold, wind, and blowing snow. The remote location makes anything that might otherwise seem trivial an incredible challenge.

In this harsh area, the RPAS conducted periodic surveys, and the AWRIS continuously monitored the harsh weather, providing critical situational awareness. Each has its advantages and challenges. For the most part, the ADOT&PF avalanche practitioner was able to operate the RPAS, maintain the ARWIS system, and successfully collaborate in this project. The M&O staff were also able to demonstrate to NOAA weather forecasters the weather dynamics at the pass that had not been seen before through the RPAS surveys and ARWIS continuous environmental monitoring. More accurate weather forecasts for Atigun Pass can benefit ADOT&PF.

For such a difficult location for monitoring avalanche conditions, we would like to see more technological and information solutions, with robust in situ reporting, to aid the avalanche forecaster, the M&O staff, and their leadership.

Chapter 7 REFERENCES

Adams, M.S., Bühler, Y. and Fromm, R., 2018. Multitemporal accuracy and precision assessment of unmanned aerial system photogrammetry for slope-scale snow depth maps in Alpine terrain. *Pure and Applied Geophysics*, *175*, pp.3303-3324.

Anchorage Daily News (2014), "50-mile stretch of highway out of Valdez closed by avalanches" February 28 https://www.adn.com/alaska-news/article/50-mile-stretch-highway-out-valdez-closed- avalanches/2014/01/26/

Bell, M.J., 1993. Wind pumping in a snow pack related to atmospheric turbulence.

Belz, N., McCormack, E. and Pacific Northwest Transportation Consortium, 2021. *Guidelines for Using Photogrammetric Tools on Unmanned Aircraft Systems To Support the Rapid Monitoring of Avalanche- Prone Roadside Environments* (No. 2019-M-UW-2). Pacific Northwest Transportation Consortium (PacTrans)(UTC).

Bianchi, F.M., Grahn, J., Eckerstorfer, M., Malnes, E. and Vickers, H., 2020. Snow avalanche segmentation in SAR images with fully convolutional neural networks. *IEEE Journal of Selected Topics in Applied Earth Observations and Remote Sensing*, *14*, pp.75-82.

Bühler, Y., Adams, M.S., Stoffel, A. and Boesch, R., 2017. Photogrammetric reconstruction of homogenous snow surfaces in alpine terrain applying near-infrared UAS imagery. *International Journal of Remote Sensing*, *38*(8-10), pp.3135-3158.

Daily News-Miner (2017), "Avalanche closes Dalton Highway at Atigun Pass; 4 trucks hit" February 28. https://www.truckersnews.com/videos/article/15057374/four-tractor-trailers-get-caught-in-an-alaskan- avalanche

Eberhard, L.A., Sirguey, P., Miller, A., Marty, M., Schindler, K., Stoffel, A. and Bühler, Y., 2021. Intercomparison of photogrammetric platforms for spatially continuous snow depth mapping. *The Cryosphere*, *15*(1), pp.69-94.

Eker, R. and Aydın, A., 2019. Evaluation of snow avalanche hazard on the highway using high resolution UAV data: case of the Erzurum-Çat-Karlıova highway, Turkey.

Filhol, S. and Sturm, M., 2015. Snow bedforms: A review, new data, and a formation model. *Journal of Geophysical Research: Earth Surface*, *120*(9), pp.1645-1669.

Hancock et al. (2020)

Kobayashi, D., Ishikawa, N. and Nishio, F., 1988. Formation process and direction distribution of snow cornices. *Cold Regions Science and Technology*, *15*(2), pp.131-136.

Lee, S., Park, J., Choi, E. and Kim, D., 2021. Factors influencing the accuracy of shallow snow depth measured using UAV-based photogrammetry. *Remote Sensing*, *13*(4), p.828.

Maier, K., Nascetti, A., Van Pelt, W. and Rosqvist, G., 2022. Direct photogrammetry with multispectral imagery for UAV-based snow depth estimation. *ISPRS Journal of Photogrammetry and Remote Sensing*, *186*, pp.1-18.

Naito, A. and Kobayashi, D., 1986. Experimental study on the occurrence of cornice, Low Temperature Science, Physics, 44, 91–101, 198.

Nolan, M., Larsen, C. and Sturm, M., 2015. Mapping snow depth from manned aircraft on landscape scales at centimeter resolution using structure-from-motion photogrammetry. *The Cryosphere*, *9*(4), pp.1445-1463.

NRCS 2024

Redpath, T.A., Sirguey, P. and Cullen, N.J., 2018. Repeat mapping of snow depth across an alpine catchment with RPAS photogrammetry. *The Cryosphere*, *12*(11), pp.3477-3497.

Se, S.H., Ji, W.G., Jeong, J. and Kim, K.H., 2023. Wind tunnel experiment and thermodynamic modeling for dry-snow accretion on a heated surface. *International Journal of Heat and Mass Transfer*, *207*, p.123990.

van Herwijnen, A. and Fierz, C., 2014. Monitoring snow cornice development using time-lapse photography. In *Proceedings of the International Snow Science Workshop* (pp. 865-869).

Vogel, S., Eckerstorfer, M. and Christiansen, H.H., 2012. Cornice dynamics and meteorological control at Gruvefjellet, Central Svalbard. *The Cryosphere*, *6*(1), pp.157-171.

Yu, H., Li, G., Walter, B., Lehning, M., Zhang, J. and Huang, N., 2023. Wind conditions for snow cornice formation in a wind tunnel. *Cryosphere*, *17*(2), pp.639-651.

BIBLIOGRAPHY

Haddad, A., Hendrikx, J., Humstad, T., Solbakken, E., Johnson, J. and Sproles, E.A., QUANTIFYING THE IMPACT OF NEW DATA STREAMS IN AVALANCHE FORECASTING.

Masný, M., Weis, K. and Biskupič, M., 2021. Application of fixed-wing UAV-based photogrammetry data for snow depth mapping in alpine conditions. *Drones*, *5*(4), p.114.

McCarty, D., Brown, R.L. and Montagne, J., 1986. Cornices: their growth, properties, and control. In *International Snow Science Workshop, Lake Tahoe* (pp. 41-45).

Miller, Z.S., Peitzsch, E.H., Sproles, E.A., Birkeland, K.W. and Palomaki, R.T., 2022. Assessing the seasonal evolution of snow depth spatial variability and scaling in complex mountain terrain. *The Cryosphere*, *16*(12), pp.4907-4930.

Revuelto, J., Alonso-Gonzalez, E., Vidaller-Gayan, I., Lacroix, E., Izagirre, E., Rodríguez-López, G. and López-Moreno, J.I., 2021. Intercomparison of UAV platforms for mapping snow depth distribution in complex alpine terrain. *Cold Regions Science and Technology*, *190*, p.103344.

Water Supply and Snow Survey Program, Natural Resources Conservation Service, United States Department of Agriculture. Atigun Pass – Air, Water, and Soil Plots. Available online. Accessed [02/22/2024] https://nwcc-apps.sc.egov.usda.gov/awdb/site-plots/POR/SNWD/AK/Atigun%20Pass.html